Investigating the effect of stabilising Hypoxia Inducible Factor 1-alpha on Estrogen Receptor target genes.

Jane Elizabeth Nesworthy

MSc (by research)

University of York

Biology

September 2023

Abstract

The estrogen receptor (ER) is a master regulator and driver of 70% of breast cancers, making the ER a primary therapeutic target. Hypoxia, common in ER+ breast tumours, plays a central role in tumour development and response to treatment. Hypoxia inducible factor-1-alpha (HIF-1α) is a transcription factor which when stabilised by dimethyloxalylycine (DMOG), robustly reprogrammed oncogenic ER binding, a preliminary finding by the Holding lab via ChIP-seq analysis.

Building on this ChIP-seq analysis, this project aimed to investigate GREB1, PS2 and CASC4 protein alterations in response to DMOG by western blot analysis. Then to investigate this on a transcriptional level, we performed RT-qPCR of *GREB1, PS2* and *CASC4*. Using proximal ligation assay (PLA), we aimed to confirm that HIF-1α and ERα are within proximity (40nm), to suggest a protein-protein interaction. All assays were performed using MCF-7 and T47-D ER+ breast cancer cell lines. The hypothesis was that loss and/or gain in ER binding in response to HIF-1α stabilisation will result in an increase or decrease respectively of the nearby gene's transcripts and protein products based on changes in ER binding.

Western blot analysis showed a potential increase in GREB1 protein in each cell line. In addition, an increase in PS2 protein in MCF-7 cell lines. These results did not support the initial hypothesis. Changes in CASC4 protein were inconclusive. RT-qPCR analysis of *GREB1, PS2* and *CASC4* show that mRNA alterations are cell line-specific in response to 2mM DMOG. *PS2* mRNA was decreased upon HIF-1α

stabilisation in both cell lines, and *CASC4* mRNA was increased on HIF-1α activation, both results supporting the initial hypothesis. PLA data was inconclusive, Optimisation conditions of each assay established in this project provides the grounding for continuation of assays to establish additional data for more reliable results.

Table of Contents

List of Tables

List of Figures

Acknowledgements

This achievement is dedicated to my parents. My Mam who has given me sunshine every single day. My Dad who has moved any mountain that's gotten in my way.

To Kyle, my boyfriend. See how much we have achieved together. You are my home and happiest place.

My Grandparents, who are a part of my every achievement. I know you would all be proud.

Auntie Jane, because not just anyone can be one... You're always there to keep me fabulous.

Rosie & Sunny. You've been there for me more than you'll ever know.

All of my friends and family (and family arriving soon).

I would like to express my deepest gratitude to Andy, who has been an exceptional supervisor to this project, and has shown full support from start to finish.

I’m extremely grateful to Nia, as my co-supervisor, who has offered me great support and many words of encouragement.

I’m also thankful to Will and Katherine who kindly agreed to be members of my thesis advisory panel. Thank you for sharing your extremely valuable knowledge with me and supporting my project.

This endeavour would not have been possible without Susanna, who provided me with my lab training and spent much of her time working alongside me on this project.

Special thanks to Weiye, who was also an asset to my lab training and always on hand to help and support.

Declaration

I declare that this thesis is a presentation of original work, and I am the sole author. This work has not previously been presented for a degree or other qualification at this University or elsewhere. All sources are acknowledged as references.

1. Introduction

1.1 Hypoxia is a Key Feature of the Cancer Tumour Microenvironment

Healthy mammalian tissue has a physiological oxygen (0_2) level of 2-6% 0_2, depending on tissue, a level we term in physoxia. This level contrasts with normoxia, the term used to describe the up to 18% 0_2 we typically use in laboratory cell culture (Alva et al., 2022). In healthy tissues, normal aerobic metabolic process can occur, and as the tissue develops, hypoxia sensing ensures the development of new vasculature to maintain homeostasis of the tissue, including 0_2 at physiological levels. Within cancer tumours, however, the highly proliferative nature of the cells causes the 0_2 levels within tumour masses to become impaired due to obstruction and compression of the surrounding vasculature. Consequentially, there becomes a very limited 0_2 supply particularly to the centre of the tumour (Masoud & Li., 2015). To adapt to such a hostile microenvironment, cancer cells form a vasculature of their own to ensure they can still meet their nutrient and 0_2 needs to continue proliferation at rapid rates. However, these neo-vasculature structures are low in pericyte coverage with loose inter-endothelial cell junctions making them leaky, which in turn increases interstitial fluid pressure. This adaptive feature of cancer tumours plays a key role in defining the tumorigenic microenvironment characterised by hypoxia (Schaaf, Garg and Agostinis., 2018, Azzi, Hebda and Gavard., 2013).

1.1.1 HIF-1 is a Master Regulator of Hypoxia Sensing

Hypoxia inducible factor-1 (HIF-1) is comprised of HIF-1α and HIF-1β subunits. HIF-1α is 0_2 sensitive and therefore only present in abundance under hypoxic conditions, whereas HIF-1β is constitutively expressed within the nuclei (Smythies et al., 2019). The HIF-1α subunit has an 0_2 dependent degradation domain (ODDD) overlapping an NH_2 terminal (N-TAD) in its structure, a distinctive difference from its fellow subunit HIF-1β. It is the N-TAD transactivation domain, that is responsible for the stabilisation of HIF-1α in hypoxia (Masoud and Li., 2015).

As illustrated by Figure 1 below (left), In normoxia, HIF-1α is rapidly degraded within a <5-minute half-life. The ODDD is recognised as a substrate by prolyl-4-hydroxylases (PHDs) – a group of 0_2 dependent enzymes. HIF-1α becomes hydroxylated by PHDs, which in turn is recognised by the von Hippel Lindau protein (pVHL), a tumour suppressor protein responsible for the negative regulation of HIF-1α. At this point, HIF-1α is tagged for ubiquitination, followed by proteasomal degradation (Yang, Harris and Davidoff., 2018, Masoud and Li., 2015).

As illustrated by Figure 1 below (right) under hypoxic conditions where molecular 0_2 level ranges from <0.1 mmHg to 15mmHg, PHDs do not have the required levels of substrate to be catalytically active; thus, HIF-1α cannot be hydroxylated and the protein is stabilised within the cell (Rashid et al., 2021). Stable HIF-1α translocates to the nucleus and associates with HIF-1β (Smythies et al., 2019) to form the HIF-1 heterodimeric transcription factor. In its heterodimeric form, the HIF-1α/β complex binds to hypoxia response elements (HRE) encoded within the DNA. At these sites,

the transcription factor coordinates the induction of genes responsible for erythropoiesis, angiogenesis, metabolism, and apoptosis (Lee, Chandel and Simon., 2020) each of these processes play a crucial part of the cell's adaptive response to hypoxia (Rashid et al., 2021, Schödel et al., 2011).

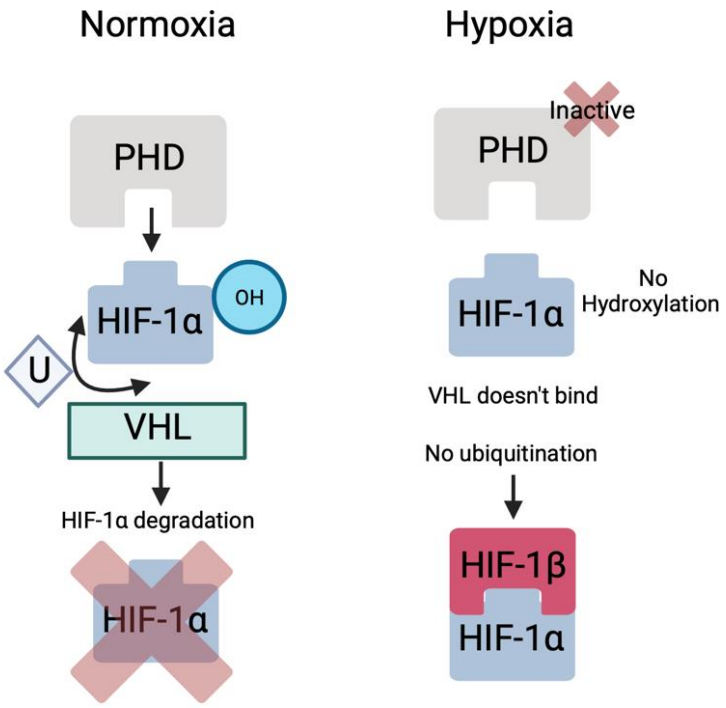

Figure 1 - HIF-1α degradation (left), HIF-1α stabilisation and comprising with HIF-1 (right).

(Figure 1 Created with BioRender.com) HIF-1α is regulated by 0_2 concentration (figure 1, left). Conditions are considered normoxic at approximately 20% 0_2. In normoxic conditions, HIF-1α is degraded rapidly, regulated by VHL. Firstly, PHD facilitates the binding of molecular 0_2 molecules to specific proline residues on HIF-1α. VHL binds to the then hydroxylated HIF-1α, triggering a group of proteins, responsible for the ubiquitination of HIF-1α. At this point, HIF-1α has been targeted

for proteasomal degradation. Under hypoxic conditions (figure 1, right), PHD is inactivated. Therefore, subsequent hydroxylation cannot occur, VHL is unable to bind to HIF-1α to target for ubiquitination and proteasomal degradation. Stabilised HIF-1α then translocated to the nucleus of the cell where it dimerises with HIF- β (Pecorino et al., 2021).

1.1.2 HIF-1 Plays a Key Role in Cancer Pathogenesis

HIF-1 is the central mediator of hypoxic survival pathways involved in cancer pathogenesis (Masoud & Li., 2015). The vascular endothelial growth factor (VEGF) is transcriptionally induced by HIF-1, which in-turn stimulates pathological angiogenesis in solid tumours (Pereira et al., 2014). Angiogenesis is essential for breast tumor survival, as the cells must be in proximity of 100-200μm of vasculature to facilitate 0_2 diffusion (Pecorino et al., 2021). VEGF is a prognostic factor of various cancers including breast cancer (Ruohola et al., 1999).

HIF-1 also helps to increase glucose transportation to tumour cells. HIF-1 coordinates an adaptive response known as the Warburg effect at a transcriptional level. The Warburg effect describes the phenomenon whereby the oxidative phosphorylation method is shifted to the less efficient – glycolysis, driving tumor cells to consume more glucose than a healthy mammalian cell. Thus, the tumor cells can meet higher energy requirements (Liberti & Locasale., 2016, Semenza., 2013).

Further, HIF-1 promotes the metastatic pathway into tissues that have higher 0_2 concentration by transcriptionally activating oncogenic growth factors including: transforming growth factor beta3 (TGF- β3) and epidermal growth factor (EGF) (Masoud and Li,. 2015).

1.1.3 Challenges of HIF-1α as a Therapeutic Target

HIF-1 ‘s role as the master regulator of multiple aggressive cancer hallmarks including metabolic alterations (Warburg effect) and oncogene activation (TGF- β3 and EGF) has led to much interest in to targeting HIF-1 therapeutically in cancer. In addition, its association with breast cancer drug resistance make HIF-1 a protein of specific interest for treating breast cancer (Wigerup, Påhlman and Bexell., 2016). However, the ubiquitous nature of HIF-1 presents a challenge in the development of a drug which will directly or indirectly target HIF-1 protein-protein interactions if we are to avoid disturbance of other healthy metabolic pathways (Masoud and Li., 2015). For example, some studies have suggested the off-target characteristics of HIF-1α inhibitors may cause toxicity in normal tissues, limiting their clinical use. This Identifies a research area for HIF-1α inhibitors, specific to cancer cells to minimise toxicity (Soni and Padwad., 2017). An additional challenge is understanding the multiple signalling pathways involved in the regulatory process of HIF-1α. An example of this being Akt and MAPK pathways. Therefore, to target HIF-1α, there needs to be a more comprehensive understanding of the factors involving regulation and signalling pathways which control HIF-1α activity (Masoud and Li., 2015).

1.2 Breast Cancer

Breast cancer is the most diagnosed cancer in women, and the major cause of female cancer related deaths worldwide (Wagner et al., 2019). Patients who are considered part of the breast cancer risk group are above the age of 50, and patients with a positive family history. Additional risk factors include, late pregnancies, hormone replacement therapies including estrogen and carrying excess adipose tissue post menopause (Valko-Rokytovská et al., 2021). Prognostic predictions are made in the clinical setting by immunochemistry testing (IHC). IHC can detect Human epidermal growth factor (HER2) and ER proteins which are the key pathological protein biomarkers for disease classification. Knowing the patient's ER status provides opportunity for targeted interventions as part of their treatment regime (Calhoun & Collins., 2015, Li et al., 2015).

1.2.1 Estrogen Receptor Positive Breast Cancer

The most common sub-type of breast cancer is estrogen receptor positive (ER+), accounting for approximately 75% of breast cancer diagnosis. ER+ breast cancer is characterised by ER presence within the breast cancer cells. (Bardia et al., 2019). Identifying ER presence in breast cancer cells, determines treatment options as well as prognosis. The slow growing nature of ER+ breast cancer tumors, means the cancer is typically more responsive to hormone targeting therapy, designed to target the ER signalling pathway (Waks and Winer., 2019).

1.2.2 Estrogen Receptor-α is a Transcriptional Regulator

Estrogen receptor-α (ERα) is part of the sex steroid hormone superfamily and plays a critical role in breast cancer development. Steroid hormones can enter through plasma membrane, allowing ERα to function as a nuclear receptor (Hanker, Sudhan and Arteaga., 2020). On binding intracellular estrogen, the inactive ER changes confirmation and the active form is released from heat shock proteins and dimerises. The now active ER then binds estrogen response elements (EREs) at sites of open chromatin (see figure 2 below). At these sites, it recruits a complex of epigenetic and transcriptional regulators to activate gene expression. In normal tissue, the transcriptional programme plays a key role in a diverse array of functions – for example, the menstrual cycle in females, brain function and the development of breast tissue, and it plays a role in inflammation (Fuentes and Silveyra., 2019).

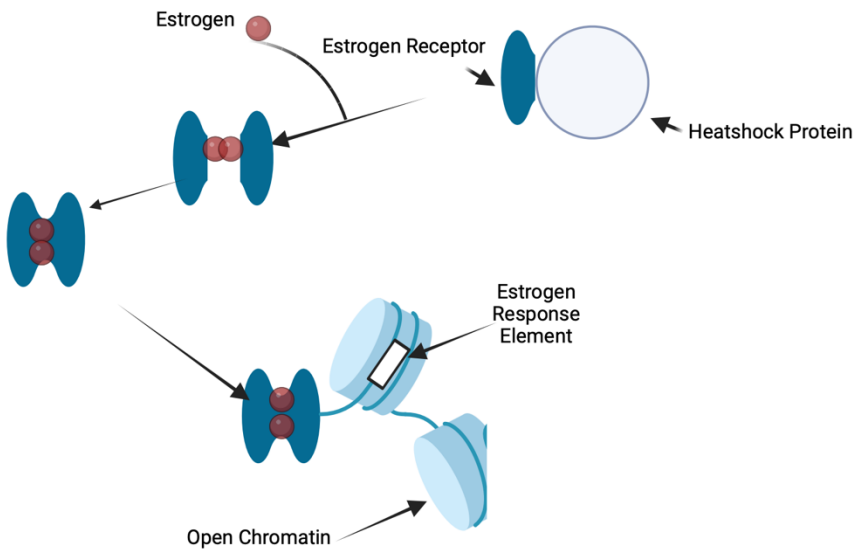

Figure 2 - Nuclear ER signalling pathway

(Figure 2 Created with BioRender.com) Following activation estrogen binds to ER, which then translocates to the nucleus of the cell. Within the nucleus, hormone bound ER, binds to ERE to regulate estrogen responsive genes.

1.2.3 ERα is a Key Therapeutic Target for Breast Cancer

75% of all breast cancers are driven by ERα in response to estrogen. The critical role of ERα in tumour growth has led to the protein becoming an important therapeutic target in breast cancer therapy development (Yang et al., 2015). The following are the main treatment strategies for targeting estrogen action. Tamoxifen is an example of a competitive inhibitor which has been used to treat ER+ breast cancer in pre-menopausal patients (Mishra et al., 2021). Additionally, ER modulators (known as SERMs) which antagonise estrogen action (Pecorino et al., 2021). Further, fulvestrant, which is a selective estrogen receptor degrader (SERD). Fulvestrant differs from tamoxifen and other aromatase inhibitors, because rather than blocking estrogen binding, it causes ER degradation by the cell's own protein degradation machinery (Nathan and Schmid., 2017). Also, the idea that drugs can interfere with estrogen synthesis to provide a treatment option for post-menopausal ER+ breast cancer patients is an additional therapeutic target (Sestak et al., 2018, Pecorino et al., 2021).

1.3 The ERα HIF-1α Crosslink

1.3.1 HIF-1 α's Key Role in ER+ Breast Cancer Requires a Deeper Level of Understanding

Cancers where high levels of HIF-1α have been identified are associated with premature relapse, metastasis, and higher rates of mortality due to HIF-1α's role in the hypoxic stress response (Liu, Semenza and Zhang., 2015). Further, the most aggressive phenotypes of breast cancer tend to express high levels of HIF-1α (Masoud and Li., 2015). Such breast tumours tend to be larger due to rapid cell proliferation rates facilitated by HIF-1 adaptive pathways and more susceptible to lymph node metastasis (Yang, Harris and Davidoff., 2018). Problematically, breast cancer tumours expressing HIF-1α are associated with chemotherapy resistance (including to tamoxifen) as well as resistance to neoadjuvant, primary, and chemo-endocrine therapy (Yang, Harris and Davidoff., 2018). Through deeper mechanistic understanding of HIF-1α's ability to reprogramme the oncogenic ER pathway, therapeutic methods could be developed to treat patients for whom hypoxia driven metastatic reoccurrence is currently untreatable.

1.3.2 HIF-1α Leads to Drug Resistance in ER+ Breast Cancer

Despite treatment showing effective results in the first instance manifesting as tumor shrinkage or disease stabilisation, ER+ breast cancers are susceptible to genomic evolution. This ultimately leads to chemoresistance (Reinert et al., 2018). Therefore, opportunities to prevent or treat endocrine resistant and metastatic ER+ breast cancer are of considerable interest in resolving a clear medical need. HIF-1α activates the PI3K/AKT/mTOR signalling pathway by upregulating growth factor and

cytokine expression, promoting increased cell proliferation and survival. Studies have implicated this HIF-1α activated pathway in resistance to endocrine therapy and chemotherapy in breast cancer (Lee, Golinska and Griffiths., 2021). Another mechanism by which HIF-1α promotes drug resistance in ER+ breast cancer is estrogen signalling regulation, which is closely explored in this project. Upregulation of ER expression and co-regulators of ER causes an increase of ER signalling and therefore creates resistance to endocrine therapy (Yang et al., 2015).

1.3.3 ERα and HIF-1α have Known Interactions

As established, both HIF-1α and ERα play a critical role in pathogenesis of ER+ breast cancer. Moreover, the transcription factors have known interactions with each other – it was identified 24 years ago, that estradiol, an estrogenic steroid, caused an increase of *VEGF* mRNA in breast cancer cell lines. Therefore, it can be concluded that estrogen induction of *VEGF* mRNA expression, possibly contributed to neo-angiogenesis in addition to the known coordinated by HIF-1 (Ruohola et al., 1999). Since then, additional studies have explored this interaction – In 2001 stimulation of estrogen in MCF-7 and T47-D breast cancer cell lines showed an increase in *VEGF* mRNA in normoxia. However, in conditions of 0.1% $0_{2,}$ plus the estrogen stimulation, had an additive effect of *VEGF* mRNA in comparison to normoxia (Maity et al., 2001).

In more recent years, additional clarity towards the relationship between HIF-1α and ERα has come to light. (Yang et al., 2015) established that the *HIF-1α* gene targets ERα protein. ERα as a HIF-1α target, was concluded by the analysis of a subgroup of genes upregulated by hypoxia, and responsive to both estrogen and 0_2. Therefore, these genes contain a hypoxic response element (HRE) as well as a ERE. In the same study, it was found that HIF-1α regulation may be responsible for estrogen signalling, when ERα function is reduced by endocrine therapy (Yang et al., 2015). For example, when a hormone therapy drug (e.g., tamoxifen) successfully reduces ERα function, stabilised HIF-1α compensates as a transcription factor for compromised ERα (Yang, Harris and Davidoff., 2018). As a result, the tumour is no longer responsive to treatment. HIF-1α function is therefore associated with the most aggressive forms of ER+ breast cancer.

Based on these results, it is apparent that HIF-1α can co-operate with ERα, which means it can integrate itself within the ERα oncogenic signalling pathway and thereby regulate expression of genes (Yang, Harris and Davidoff., 2018). An example of this being *KDM4B,* a gene which can be expressed by both ERα and HIF-1α. In breast cancer (possibly as well as other cancer types), *KDM4B* regulates the G2/M phase of cell cycle. Both *VEGF* and *KDM48* possess ERE and HRE elements at their genomic locus. Both genes playing a role in cell cycle progression and tumour cell proliferation in ER+ breast cancer (Yang, Harris and Davidoff., 2018). In ER+ breast cancer cells that have become resistant to endocrine therapy, regulation of *KDM48* by HIF-1α and ERα remains ongoing (Yang, Harris and Davidoff., 2018). Despite the growing evidence of gene specific interactions between HIF-1α and ERα, there is yet to be a global view of ERα /HIF-1α signalling crosstalk.

1.3.4 Preliminary findings show ERα and HIF-1α interact genome wide

The Holding lab previously identified a genome wide process where ER binding is altered in response to HIF-1α activation. This result suggests that, unlike previous examples of ERα /HIF-1α interactions where the transcription factors could compensate for each other, hypoxia instead directly affected the estrogen response. The ChIP-seq data presented as in the heatmap (figure 3) below, was generated by chemically stabilising HIF-1α within MCF-7 cells using 2mM dimethyloxalylglycine (DMOG), a cell permeable competitive inhibitor of PHD (Zhang et al., 2015).

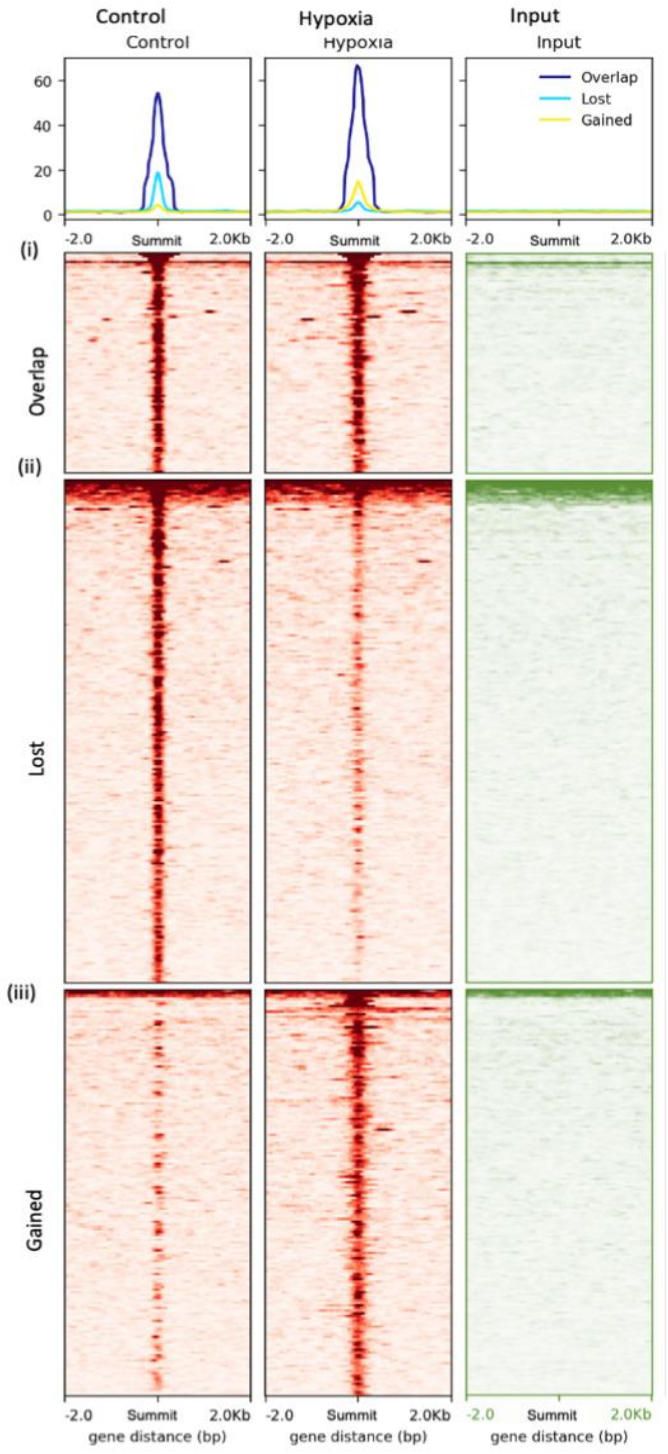

Figure 3a - HIF-1 stabilisation causes a genome-wide process where altering ER binding is visualised as a ChIP-Seq heatmap.

Peaks are aligned by the summit and ordered from highest to lowest intensity within their category. Three categories of changes in ER binding upon addition of DMOG to mimic hypoxic conditions were identified. In the first category, ER binding was maintained where peaks were called by MACS2 in both the control and DMOG treated condition. These peaks are labelled (i) overlap in data. This result is visible as equal density of the summits in the first two columns upon the heatmap. In the second category, ER binding was lost labelled (ii), this presents on the heatmap as the less dense of the peaks in the hypoxia group and these peaks were only called by MACS2 in the control conditions. For the final category, ER binding was gained upon addition of DMOG (iii), and these peaks were only called in the DMOG condition and not in the control condition. This change is visible as more density at the peak summit in the hypoxic group, compared to the control.

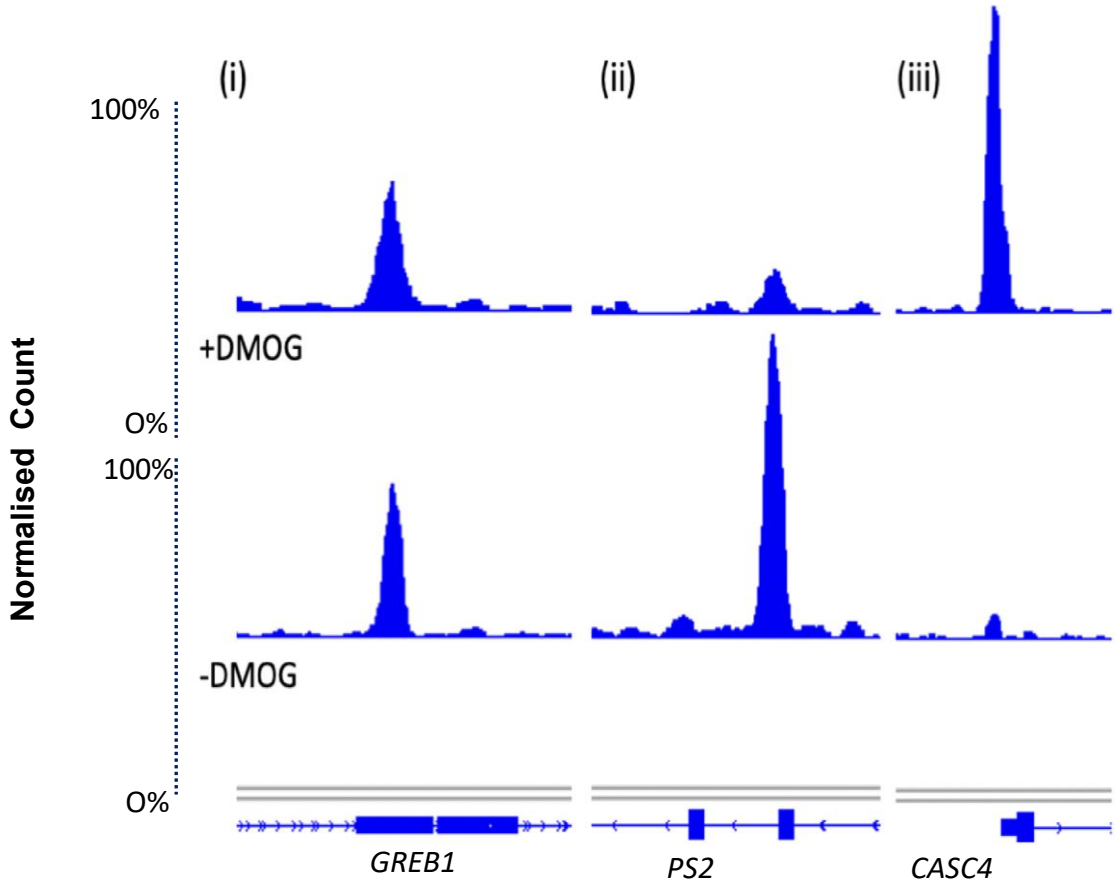

Figure 3b - Highlighted ChIP-seq data, showing three different classes of response at three ER binding sites (GREB1, PS2, and CASC4) in response to HIF-1 activation.

Here, figure 3b shows 3 examples of genomic locations which are examples of the 3 binding alterations caused by the presence of DMOG, stabilising HIF-1. An example of class (i), where there is no change in ER binding with and without DMOG is found at an enhancer in exon 3 of GREB1. Binding at the enhancer region in TMPRSS2 of the known estrogen response gene TFF1/PS2 (hereon referred to as PS2), is an example of class (ii) where there is a significant reduction of ER binding where DMOG is present. Finally, for class (iii) binding sites, there is a significant increase of ER binding where DMOG is present. The promoter of CASC4 is shown as an example of this.

1.4 Research Aims

Preliminary ChIP-seq showed that the reprogramming of ERα binding alters the expression of nearby genes. Therefore, the first aim of this project is to build upon this finding by the Holding lab by monitoring how changes in ER binding alter the protein and transcript levels of genes located near to the binding changes. The second aim of this project is to confirm if there is a detectable interaction between HIF-1α and ERα.

Hypothesis: loss and/or gain in ER binding in response to HIF-1α stabilisation will result in an increase or decrease respectively, of the nearby gene's transcripts and protein products

2. Materials and Methods

2.1 Cell Line Culture

Cells were acquired from ATCC by the Holding lab, and stocks were stored within the lab under liquid nitrogen stocks as 2 mL cryovial aliquots containing 2x10^6 cells in 50% DMSO/50% FBS. To revive cells, they were thawed at room temperature before centrifugation at 180 x g for 6 minutes. The supernatant was then aspirated, and the cell pellet was resuspended in 10 mL Dulbecco's Modified Eagles Medium-high glucose (DMEM) (Gibco) + 10% FBS (Gibco) for seeding. Typically, cells were seeded in a T75 flask (Nunc). Cells were stored and maintained in an incubator (Galaxy R+) set to 37°C, 5% $C0_2$, 4.3% 0_2.

MCF-7 human adenocarcinoma cells and T-47D epithelial cells were maintained with DMEM, purchased pre-modified to include 4500mg/L glucose, L-glutamine, sodium pyruvate and sodium bicarbonate. To the supplemented modified DMEM, I added 10% foetal bovine solution to make complete media. To perform trypsinisation of cells, they were first washed with PBS followed by with Trypsin-EDTA (0.05%) (typically 2.5ml). Trypsin as quenched using the complete medium before centrifugation at 180 x g for 5 minutes at room temperature. Cells were routinely passaged at 70% confluency and split 5:1. Cells lines were discontinued at passage 35 or above.

2.1.1 Cell Counting with haemocytometer

Cells were resuspended in an appropriate volume of complete media to prevent aggregation following trypsinisation. 10µl was transferred to a haemocytometer (Neubauer CE, Hirschmann EM Techcolor). If cell numbers were significantly higher than 200 cells/square or lower than 100 cells/sequence the cell suspension was diluted or concentrated as needed. The cells were counted across 4 outer squares and divided by 4 to obtain an average. The slide was viewed with a Nixon TMS inverted microscope using a 10X objective. The number of cells within 4 of the larger squares on the haemocytometer were counted using a manual cell counter. The average of the 4 squares were multiplied by 10^4, to give the average number of cell/ml in the suspension.

2.1.2 Seeding and Collection of Cells in Preparation for Western Blot Assay

Both MCF-7 and T47-D cells were seeded into 6-well plates at a seeding density of 2 x 10^4 cells per cm^2. After 24 hours, cells had adhered to the base of the wells. At 70% confluence the cells were treated with 2mM DMOG (21µl of 285mM DMOG stock in 3ml media per well to make 2mM DMOG) or DMSO (0.7%) as a vehicle control. Cells were returned to the incubator set to 37°C, 5% $C0_2$, 4.3% 0_2 for 17 hours.

2.1.3 Seeding and Fixing of Cells in Preparation for Proximity Ligation Assay

MCF-7 and T47-D cells were seeded onto an 8-chamber slide (ThermoFisher/ 154534) at 2 x 10^4 cells per chamber. Once cells reached an approximate 70% confluency, the cells were washed with PBS at room temperature then fixed with 400µl ice-cold methanol. The fixed cells were then either used after 5 minutes for PLA assay or stored at -20°C for up to 2-weeks with no significant change in the results seen.

2.1.4 Cell Culture Preparation for RNA Isolation

One 70% confluent T75 flask containing either MCF-7 or T47-D cells was washed with 10 ml PBS before undergoing trypsinisation for 5 minutes and resuspended into complete media. The cell suspension was then centrifuged (2000rpm, RT, 5 minutes). The supernatant was removed, and the cells resuspended in PBS. The cells were again centrifuged (2000rpm, RT, 5 minutes) and the supernatant removed. The washed cells were either used immediately for RNA isolation or stored at -80°C.

2.1.5 Collection of Cell Lysate for Western Blot Assay

Cells at 80% confluence in a 6-well plate were placed on ice. A 1:1 v/v dilution of 2x Laemmli buffer sample buffer (Bio-Rad) in PBS was added to each well at a volume of 200µl. 250nM Protease inhibitor (Roche) was added to each 1x Laemmli buffer dilution at 1:100 v/v. After equilibrating, wells were scraped with a pipette tip to remove and collect cell lysate. The cell lysate was transferred to a labelled Eppendorf and place on ice. The cell lysate aliquots were transferred to a fume cupboard where 6.7 µl ß-mercaptoethanol was added per 100µl of cell lysate. The reduced cell lysate was then be boiled at 95°C for 5 minutes to denature the proteins within the sample and used immediately used for gel electrophoresis or stored at -20°C.

2.2 Western Blot Assay

2.2.1 Gel Electrophoresis

Cell lysate was heated at 95°C for 5 minutes. 4-20% mini-protean TGX gels (Bio-Rad) were rinsed with distilled and sterile H_20 before being securely fitted into the tank. The wells were washed with 1x tris/glycine/SDS (100ml 10x stock (25mM Tris, 192mM glycine, 0.1% SDS) in 900ml filter sterilised dH_20) (Bio-Rad) running buffer, using a pipette to remove excess acrylamide that may interfere with the running of the bands. Once the tank was filled with the correct volume of running buffer comparative to how many gels were undergoing electrophoresis, the ladder and lysate could be loaded onto the gel respectively. The volume of lysate changed according to thickness of the gel (12 wells, 15µl, 10 wells, 40µl).

Gel electrophoresis was started at a 65V for 11 minutes to load the lysate into the stacking well evenly. The voltage was then manually increased to 100V for the remaining 50 minutes (or until the proteins were ran to an appropriate level for the experimental aim).

2.2.2 Gel Transfer

Following electrophoresis, gels were kept wet with distilled H_20. Immediately before use, nitrocellulose filter paper was pre-wet in distilled H_20 and PVDF in methanol for 5 minutes. Gels were then transferred onto the membrane using the iBlot 2® technology and iBlot 2® regular stacks following the manufacture's protocol.

Following transfer, membranes were cut using a clean scalpel to match the size of the gel or two smaller sections if staining for multiple proteins. Once the membrane was cut to size and/or sections, the membrane/s were transferred into a compatible blocking buffer solution.

2.2.3 Blocking

Membranes were transferred to lidded boxes large enough for the membranes to lie flat and covered with enough blocking buffer to prevent drying out. The membrane was then incubated in blocking buffer (either 4% milk or 3% BSA) at room temperature, whilst rocking for up to 2 hours at room temperature.

2.2.4 Primary Antibodies

A dilution of primary antibody was made up in 10ml of blocking buffer using the concentrations stated in table 6. Membranes were incubated with primary antibodies whilst gently rocking overnight at 4°C.

2.2.5 Wash Step

Following overnight incubation, primary antibody solution was stored at -20°C for reuse. Membranes were covered with 0.01% dilution of Tween 20 in PBS (wash buffer) in blocking buffer and allowed to rock for 15 minutes at room temperature. The wash buffer was removed and replaced for 3 more 15-minute washes (total wash time 1 hour).

2.2.6 Secondary Antibodies

10ml of a 1/10,000 dilution of secondary-HRP anti-rabbit IgG antibodies was added to the membrane and incubated whilst rocking for 1 hour at room temperature.

2.2.7 Removal of Secondary Antibodies

Secondary antibody solution was discarded, and membranes were covered with 0.01% wash buffer v/v in distilled H_2O for 15 minutes whilst rocking at room temperature. The wash buffer was removed and replaced to provide two more 15-minute washes.

The membranes were then rinsed in PBS for 5 minutes while rocking at room temperature. The PBS rinse was repeated once more.

2.2.8 ECL Imaging

A 1:1 dilution of ECL reagent (detection reagent 1 peroxide solution (Pierce) in luminol enhancer solution (Pierce)) was rinsed over the membrane for at least 1 minute using a pipette. (SuperSignal™ West Pico PLUS was used to detect smaller proteins such as PS2). The blot was then visualised using the iBright (ThermoFisher) according to the manufactures protocol. In brief, using the chemiblots function of the iBright, 3 images of the membrane were taken, and membrane overlay was applied. Images were then saved as TIFF.

2.2.9 Image analysis using ImageJ

All image analysis was performed using imageJ (windows version, bundled with 64-bit Java) (Rasband, W.S., ImageJ, U. S. National Institutes of Health, Bethesda, Maryland, USA, https://imagej.nih.gov/ij/, 1997-2018.) The rectangle function in ImageJ can be used to quantify the intensity of a region in a western blot image. The rectangle function was applied to an area of the image large enough to quantify the whole of each band being analysed. Values were obtained for both the protein of interest and for the loading control, GAPDH. The intensity was then normalised to the GAPDH loading control.

2.3 Proximal Ligation Assay

2.3.1 Blocking and Primary Antibodies

Methanol was removed from each chamber of the plate. The cells were then rinsed with 500µl PBS three times per chamber. The chamber walls were carefully removed. Any excess glue was carefully removed using a cotton swab.

2 drops of Duolink® blocking solution was added to each sample well. The 8-well slides were then transferred to a pre-prepared humidity chamber (dampened blue roll in metal tin with lid) incubated for 1 hour at 37°C. 35µl of primary antibody diluted in Duolink® antibody diluent was added per sample well, this was left in overnight incubation, in a humidity chamber at 37°C.

2.3.2 Wash Buffer

Following overnight primary antibody incubation, slides were washed with wash buffer A (Duolink® starter kit) for 20 minutes at room temperature, changing the wash buffer every 5 minutes.

2.3.3 PLA probes

35µl of 1:5 v/v dilution of PLUS and MINUS PLA probes in Duolink® antibody diluent was added to each well and left to incubate at 37°C in a pre-prepared humidity chamber for 1 hour.

Slides were then washed with wash buffer A for 20 minutes at room temperature, changing the wash buffer every 5 minutes.

2.3.4 Ligation

A 1:5 dilution of 5x Duolink® ligation buffer in sterile deionized water was created. Ligase was then added to 1x ligase at a 1:40 v/v dilution. 35µl of ligation buffer plus ligase was added to each well and returned to 37°C incubation in a humidity chamber for 30 minutes.

2.3.5 Amplification and Polymerisation

In an environment with reduced light to avoid bleach of the fluorophores, a 1:5 dilution of 5x Amplification Buffer (Duolink® starter kit) was made in deionized water. Polymerase (Duolink® starter kit) was added to the 1x amplification buffer at a 1:80 v/v dilution. 35µl of Polymerase/Amplification buffer (Duolink® starter kit) was added to each well. The wells were returned to 37°C incubation in a humidity chamber for 100 minutes.

2.3.6 Wash Buffer

Slides were washed by being submerged with 10 mL wash buffer B for 20 minutes on a table rocker, replacing wash buffer 10 minutes. Then, slides were washed with 0.01% wash buffer B for 1 minute. Wash buffer B was tapped off the slides, and a

drop of Duolink® Dapi was added to each well before a cover slip was applied to the top of the slides.

2.3.7 Imaging

Slides were imaged using the Confocal LSM780 (Zeiss). Slides were viewed on a x63/ 1.4 oil objective lense. The following settings were used to capture the images: 405nm laser excitation > 410-550nm emission for DAPI and 561nm laser excitation > 566-697nm emission for Alex 555.Scanning mode was set to plane. Pinhole sizes were set as track 1 Ch1 89µm, track 2 Ch2 89µm.

2.3.8 Image analysis

All image analysis was performed using ImageJ software [software (NIH) (Rasband, W.S., ImageJ, U. S. National Institutes of Health, Bethesda, Maryland, USA, https://imagej.nih.gov/ij/, 1997-2018.) Images were analysed in grayscale. Using the adjust threshold function to separate nuclei from the background. Binary images were used to ensure a monochromatic separation between nuclei and background. Any gaps within the nuclei were filled using the fill hole function before image analysis.

Images were then quantified using the analyse particles function. The number of nuclei/dots were recorded. The dots representing presence of HIF-1 α.

2.4 Isolation of RNA and cDNA synthesis

2.4.1 Sample Lysis and Separation of Phases

The following steps follow the TRIzol™ reagent manufactures guide. All RNA work was performed in an RNAse free environment to ensure integrity and accuracy of RNA based research. Pelleted cells were thawed at 4°C and resuspended in 1ml of TRIzol™ reagent. The resulting suspension was transferred to a clean Eppendorf. The Eppendorf was incubated for 5 minutes at 4°C.

Following this, 200µl of chloroform was added per 1ml TRIzol™ reagent. The mixture was shaken vigorously by hand to mix for 3-4 minutes, then incubated for 2 minutes at 4°C. The sample was centrifuged for at 12,000 x g at 4°C for 15 minutes. Following centrifugation, the aqueous phase was transferred by pipette to a clean Eppendorf with care.

2.4.2 RNA Isolation

0.5ml isopropanol was added to the aqueous phase, (per 1ml TRIzol™ reagent previously used) then incubated for 10 minutes at 4°C. The sample was then centrifuged at 12,000 x g at 4°C. The supernatant was then discarded, and the RNA pellet retained in the tube. Following centrifugation, the pellet was resuspended in 1ml 75% ethanol per 1ml TRIzol™ reagent. The sample was vortexed and centrifuged for 5 minutes at 7500 x g at 4°C. The supernatant was discarded, and the pellet was air dried in the cell culture hood for 5 minutes (or until the ethanol had evaporated). The RNA pellet was then resuspended in 150µl nuclease free water.

2.4.3 Quantifying RNA using Nanodrop ND-1000

If thawing the RNA solution, this was done at 4°C. Once thawed, the samples were vortexed and placed on a rack on ice. Using a NanoDrop® ND-1000 UV-Vis Spectrophotometer (ThermoScientific) the 260/280 nm absorption ratio and concentration of RNA was recorded. A ratio > 2.0 was accepted as pure RNA.

2.4.4 Agarose gel preparation

2g of Agarose was combined with 100 mL TAE buffer. The agarose/TAE suspension was microwaved to 1-3 minutes until all agarose was dissolved (do not overboil). The agarose with 10µl syber safe DNA gel stain then allowed to cool to about 50 ^{o}C and pour into at gel tray (Bio-Rad) with gel comb in place.

Once cooled, the resulting 2% agarose gel was loaded into a gel electrophoresis tank. The gel was submerged with 1x TAE buffer. 6µl of a 1:5 dilution of 5x loading dye with RNA in nuclease free water was added per well of an agarose gel. Gel electrophoresis was run for 50 minutes at 120V.

2.4.5 Imaging of Agarose RNA Gel

The gel was imaged using iBright (ThermoFisher) according to the manufactures protocol by way of the nucleic acid function. In brief, the agarose gel was visualised on blue light and images were recorded. Gel images were saved in TIFF format.

2.4.6 cDNA Synthesis

2.4.6.1 Anneal Primers to Template RNA

The primer reaction mixture was prepared on ice in a 0.2 mL PCR tube 1µl of 100 µg/mL oligo (dT) primers (Invtrogen) was combined with 1µl 100 mM dNTP mix (Invitrogen) with a variable volume of template RNA (calculated based off nanodrop value) and a variable volume of nuclease free water (calculated to make total volume 13µl. The calculation is as follows:

750ng/ concentration of RNA (ng) = volume of RNA sample to add to reaction tube (µl)

The solution was briefly vortexed and centrifuged then heated at 65°C for 5 minutes. The reaction mixture was then incubated on ice for 1 minute.

2.4.6.2 Preparation of RT Reaction Mixture

On ice, 4µl of 5x SSIV buffer (Invtrogen) was combined with 1µl of 100mM DTT, 1µl of RNaseOUT™ recombinant RNase inhibitor and 1µl of SuperScript® IV reverse transcriptase (200 U/µL). The reaction mix was briefly vortexed and centrifuged.

2.4.6.3 RT Reaction

The Annealed primers were combined with the RT reaction mixture and incubated at 50-55°C for 10 minutes, then inactivated by incubating at 80°C for 10 minutes. At this point the cDNA could be stored at -80°C or used immediately for qPCR assay.

2.5 Polymerase Chain Reaction for Primer Validation

2.5.1 Preparation of Reaction Mixture

Polymerase chain reaction (PCR) was performed to ascertain that the primer pars were compatible in both MCF-7 and T47-D cells. 10µl of SYBR® green master mix (2x) was combined with 1µl of 20ng cDNA, 1µl of 10µM primer pair and 8µl of nuclease free water (NFW) to make a total reaction volume of 20µl.

2.5.2 Set up of Thermal Cycling Conditions

The PCR was run in fast mode and thermal cycling conditions were inputted into the PCR thermocycler (MJ research) as specified In table 1 below. PCR tubes containing the reaction mixture were briefly centrifuged and each placed into a well of the optical plate in the PCR thermocycler.

Table 1: Specification of thermal-cycling conditions from SYBR Green master mix protocol.

Instrument	Step	Temperature℃	Duration	Cycles
• step 1. • Step One plus. • 7500 fast.	AmpliTaq® fast DNA polymerase, UP activation	95	20 sec	HOLD
	Denature	95	3 sec	40
	Anneal/Extend	60	30 sec	

2.5.3 Gel Electrophoresis

An agarose gel was prepared. Following PCR, 10µl of PCR reaction mixture was combined in a new tube with 2µl 6x orange DNA loading dye (Thermo-Scientific). This was then vortexed and centrifuged. An appropriate volume of 1x TAE running buffer was poured into the tank to ensure that the agarose gel was completely submerged.

6µl of the PCR reaction mixture plus the loading dye was loaded into the wells, as well as 3µl PCRBIO ladder II (PCRBiosystems) Gel electrophoresis was run at 120V for 50 minutes.

2.5.4 Visualisation of Gel Electrophoresis

The gel was imaged using iBright (ThermoFisher) according to the manufacturer's protocol by way of the nucleic acid function of the iBright. In brief, the agarose gel was visualised on blue light and images were recorded. Gel images were saved in TIFF format.

The DNA ladder allowed for determination of molecular weight. A working primer pair would show up as bands corresponding to the expected size of the PCR product on the gel. Presence of 2 bands (a 28S and 18S band) indicates that the oligo has successfully amplified to the target DNA. If this was a success in both MCF-7 and T47-D cell line, the oligo pairs were used in subsequent qPCR analysis.

2.6 RT-qPCR Assay

2.6.1 Preparation of Master Mix and Addition of Primer Pairs

Preparation for qPCR assay was performed on ice, reagents were kept on a rack (acquired from pipette tip box which had been autoclaved). Per reaction well, 10µl of fast SYBR® green master mix (2x) was combined with, 1µl containing 20ng cDNA and 8µl of nuclease free water. The 19µl reaction mixture was briefly vortexed and centrifuged. 1µl of 10µM primer pair was then added per reaction well, the reaction mixture was vortexed and briefly centrifuged.

The reaction mixture was then aliquoted into the 96-well plate, which was then sealed and transferred to the QuantStudio™3 system. Figure 4 below shows the run summary, and QuantStudio™3 system settings used for each SYBR Green® qPCR analysis.

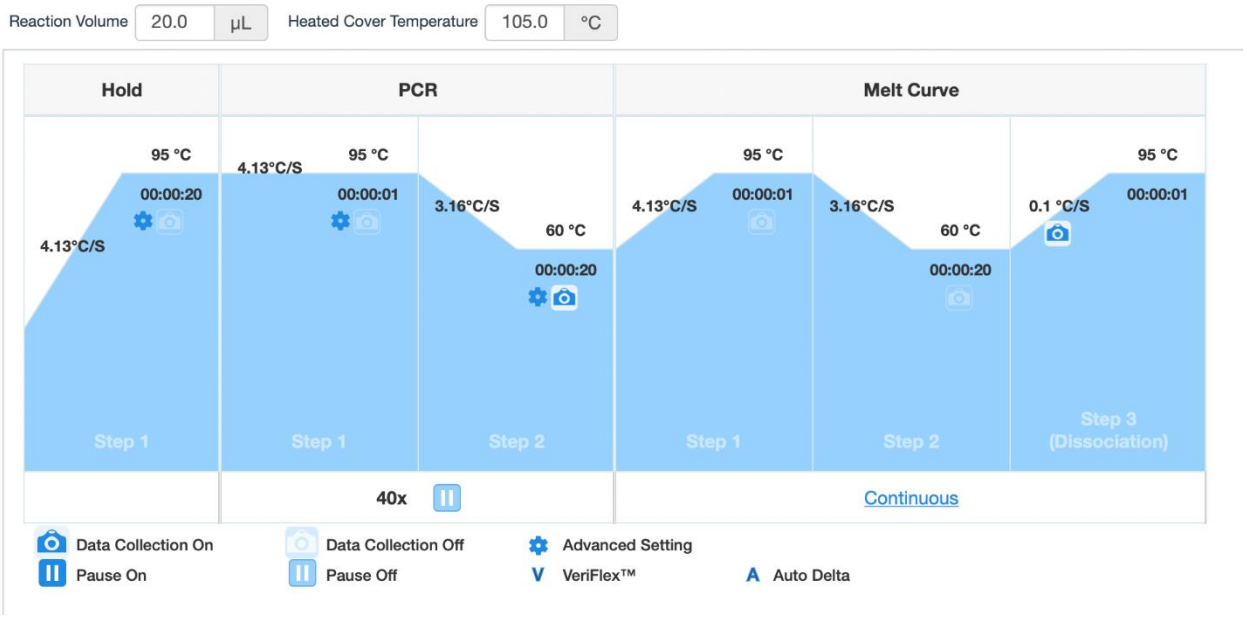

Figure 4 - QuantStudio™ 3 system set up for SYBR Green® qPCR analysis

The graph depicts each cycle of the qPCR run: hold, PCR and melt curve. This is then divided into step 1,2 and 3. At step 1, the temperature rises to 95°C, step 2 the temperature decreases to 60°C (repeated 40x), step 3, the temperature rises to 95°C again to dissociate.

Initially, the thermocycler of the QuantStudio™3 system heats to 95°C, causing the cDNA to denature. Figure 4 shows this part of the cycle during the hold step, where step 1 takes place, lasting for approximately 21 seconds. This causes the DNA helix to open, exposing two stands of DNA (templates).

Secondly, the temperature decreases to 60°C, as part of the annealing step, this can be seen in figure 4 as the PCR part of the cycle, where step 1 continues once, followed by step 2. At this point, the single stranded primers anneal to target

sequences on the single stranded DNA. Following this, DNA polymerase attaches to the now primed template strands, incorporating complementary nucleotides.

Finally, the melt curve part of the qPCR cycle, which can be seen in figure 4 as a continuation of step 1,2 and 3. The melt curve output will confirm specific PCR products. The temperature rises again to 95°C, causing DNA polymerase to extend the sequence-specific primer with complementary nucleotides to the DNA template. SYBR green then binds synthesised double stranded DNA complexed and fluoresces. This fluorescence accumulates as cycling continues and is measured at the end of each PCR cycle. The continuation of denaturing, annealing and extension cycles occurs between 35-40 times.

2.7 Data Analysis

2.7.1 Quantification of Western Blot Results

Following image analysis using ImageJ, band densities for each protein were recorded using Microsoft excel, alongside band densities of the loading control. The intensity of the target protein was then normalised to the loading control to account for variations in sample loading (see calculation below):

Target protein/ Loading control = normalised value

Data analysis was performed using the normalised data. In this case, the mean value from both technical replicates. The mean value determined final protein density.

2.7.2 Quantification of PLA

For each treatment condition (with or without DMSO) and antibody condition, images of 5 fields of view were taken. Following image analysis using imageJ, the number of nuclei and dots were recorded in Microsoft excel. The following calculation was performed to determine how many dots were present.

Total number of dots/ total number of nuclei = average number of dots/nuclei

A mean value of dots/nuclei was determined from the 5 fields of view. This value represented the average presence of HIF-1α for each treatment condition and

antibody combination. The standard deviation of the data was also recorded before formulating the data into a bar chart.

2.7.3 Quantification of qPCR data

Following the QuantStudio™3 system qPCR, the data was automatically available on the thermofisher.com data connect platform. Relevant qPCR data was exported from ThermoFisher cloud into Microsoft Excel. Cycle threshold (ct) values (listed as Cq values in ThermoFisher cloud) are automatically determined. The ct values of the control group and the experimental group was calculated once the data from each qPCR run was organised into the same spreadsheet.

Since the aim of this experiment was to compare the relative expression of three target genes: GREB1, CASC4 and T47D the delta-delta Ct (ΔΔCt) method was the appropriate calculation to use. The calculation was inputted as follows:

To calculate ΔCt = mean Ct value of target gene – Ct value of housekeeping gene

To calculate ΔΔCt = ΔCt of experimental sample (DMOG) – ΔCt control sample (DMSO)

To calculate the fold change in gene expression = 2^ (- ΔΔCt)

Following quantification, a T Test was performed using excel with the following calculation:

= T.Test (average ΔΔCt control group, average ΔΔCt treatment group, tails (2) , type (3)).

3. Results

3.1.Establishing changes in Protein Expression of HIF-1α after Chemical Induction with DMOG to mimic hypoxia.

3.1.1 Optimisation of Antibodies and Assay for Western Blotting of HIF-1α Protein in ER+ Breast Cancer Cell Lines.

Multiple HIF-1α antibodies are reported to work for the detection of HIF-1α by western blotting (Liang et al., 2018, Srinivasan and Dunn., 2011); however, none previously have been established within the lab, and we found no consensus in the literature in terms of reagents. Therefore, to provide a reliable assay for HIF-1α expression, we undertook an evaluation of which antibodies were most suitable for the analysis of HIF-1α protein expression in ER+ breast cancer cells lines, MCF-7 and T47-D cells after stimulation with 2mM DMOG to stabilise the protein. As a negative control we used unstimulated cells, and for a positive control we used hFAB™ Rhodamine anti-actin primary antibody as a positive control (12004164). The blots were carried out with both PVDF and nitrocellulose.

We tested HIF-1α antibodies from Abcam (ab51608), which showed large amount of non-specific signal in the ER+ cell lines were used. Although the antibodies showed some level of broadening upon HIF-1α stabilisation by DMOG, this was likely due to background depredated protein partial inhibition of the PHD proteins, and from post-translational modification of the HIF-1α protein. We were able to further reduce the level of degradation via the use of proteosome inhibitors and addition of MG132

inhibitors. Nitrocellulose membrane showed greater background over PVDF membrane (results shown in figure 5a below). Based on this result, we chose the Cell Signalling (P/N: 361695) antibody on PVDF for our subsequent assays.

3.1.2 HIF-1α Expression Peaks in MCF-7 Cells at 4 hours after Treatment with DMOG

Studies have shown HIF-1α and HIF-2α proteins in a context specific manner (e.g., cell type, tissue context and duration of hypoxia). It is therefore possible that HIF-1α and HIF-1α co-regulate gene expression in response to hypoxia (Roig et al., 2019). The time scale of HIF1α expression is also reported to be tissue and cell line dependant (Semenza., 2012). We therefore undertook a 24-hour time course to establish the optimum time points to investigate the effects of HIF-1α stabilisation on the expression on ERα+ target genes. The effects of hypoxia were mimicked using 2mM DMOG to chemically stabilise HIF-1α in MCF-7 cell lines for 0, 2, 4, 8, 17 and 24 hours and monitored via our established western blotting assay (figure 5a top images). HIF-1α protein stabilisation was detected at 2 hours and maximum HIF-1α expression was found at 4 hours for MCF-7.

3.1.3 HIF-1α Expression peaks in T47-D at 8 hours after treatment with DMOG

To confirm if measured timescales of HIF-1α response for MCF-7 were generalisable to other ER+ breast cancer cell lines, and to provide biological replication, we repeated the time course experiment in a second ER+ breast cancer cell line, T47-D. The effects of hypoxia were again mimicked using 2mM DMOG and lysates were

isolated for 4, 8, 17 and 24 hours (figure 5a bottom images). Analysis by western blot of HIF-1α showed, as with MCF-7 cells, a stabilisation protein within 2 hours and a peak expression of protein at 8 hours.

3.1.4 The Kinetics of the Stabilisation of HIF-1α Protein in response to DMOG is Comparable in MCF-7 and T47-D cells.

To compare the two-time course experiments, we undertook semi-quantitative densitometry of the western blot for HIF-1α for both time courses in MCF-7 and T47-D cell lines after treatment. T47-D cell lines showed denser bands for HIF-1α in response to DMOG; therefore, we normalised both time courses to the maximum intensity. Visual inspection of the profiles for each cell line (figure 5a) showed a similar profile for the HIF-1α response that the maximum for both occurred at a similar time point (4-8 hours), due to the semi quantitative nature of western blotting, and the limited number of time-points we could not conclude that the effect was significant. Nonetheless, the result confidently showed that the initial transient response of HIF-1α occurred in 8 hours or less, comparable between ER+ cell lines and that any changes in mRNA and protein expression because of DMOG treatment should be detectable within 24 hours of DMOG treatment to account for the delays caused by transcription and translation.

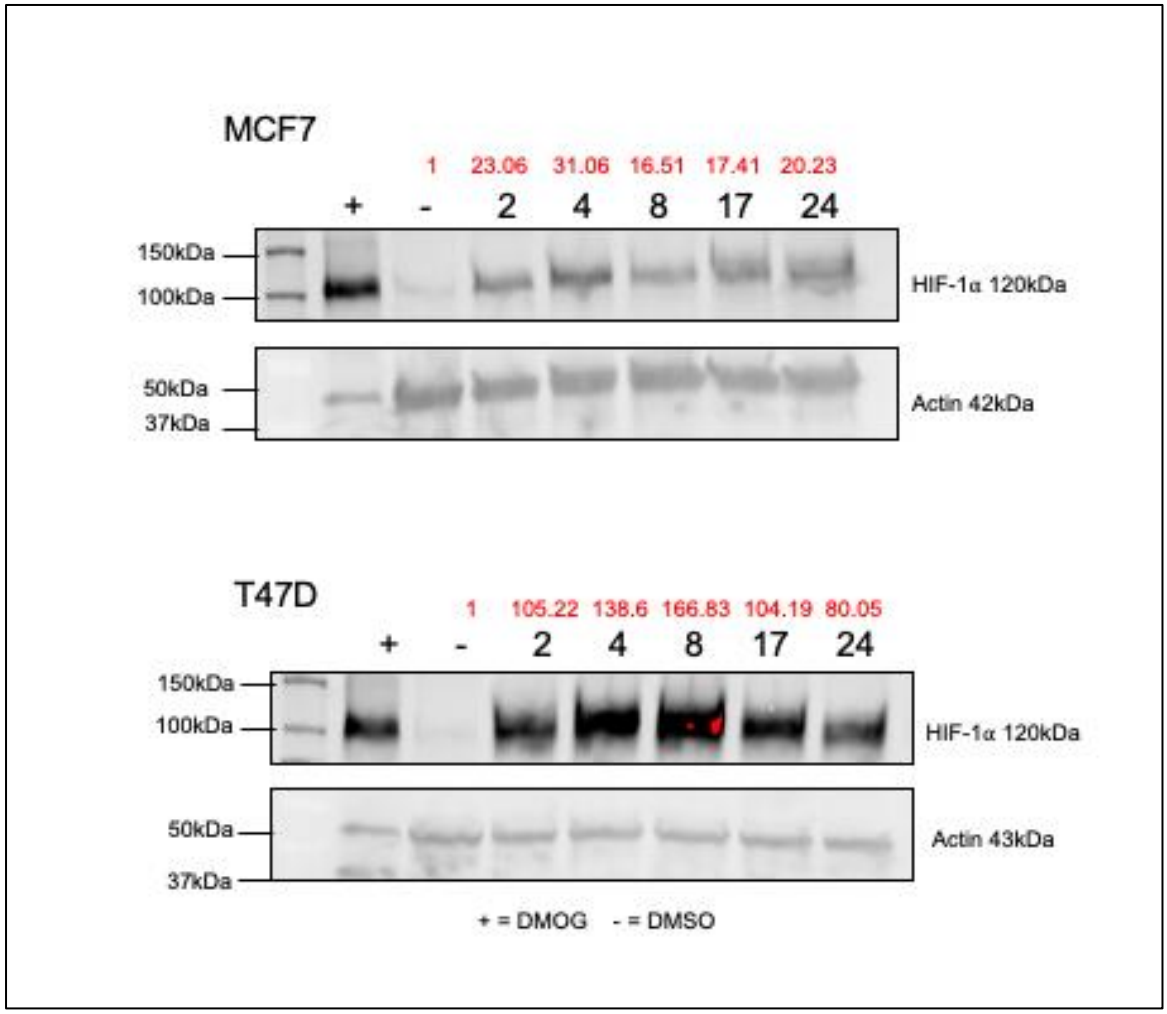

Figure 5a - 2mM DMOG increases HIF-1α protein levels in MCF-7 and T47-D breast cancer cell lines.

Abundance of HIF-1α is determined by the time incubated with DMOG. An increase of HIF-1α protein was detected within 2 hours of incubation with DMOG in both MCF-7 and T47-D cell lines, this is compared to the sample containing vehicle control only (DMSO). HIF-1α was most abundant in MCF-7 cells after 4 hours and after 8 hours in T47-D cells. Protein densities were determined from image analysis using image J software (displayed in red text above protein bands).

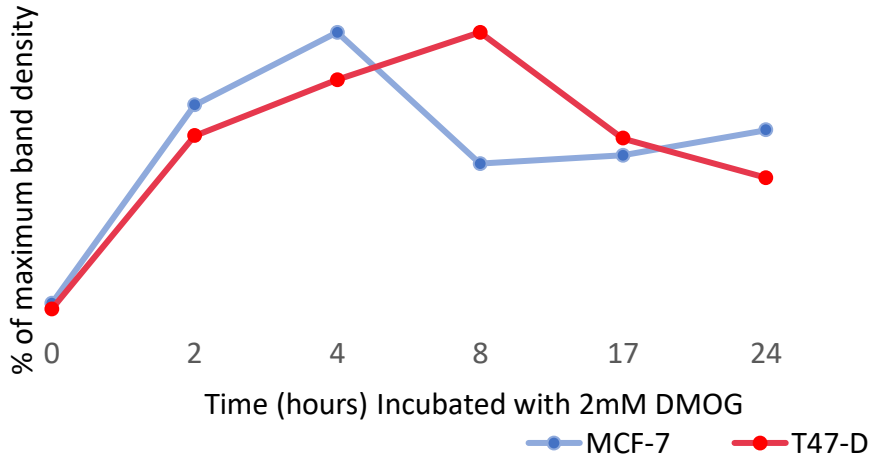

Figure 5b - Protein density of HIF-1α in MCF-7 cells (blue) and T47-D cells (red), as a percentage value of the highest protein density value of each cell line

The above graph visualises the data shown in figure 5a, showing the percentage increase of HIF-1α after 4 hours of 2mM DMOG treatment in MCF-7 and T47-D cells. The graph highlights that HIF-1α peaks at 4 hours in MCF-7 cells and at 8 hours in T47-D cells. The graph highlights the difference in HIF-1α protein density in both cell lines after 4 hours. While percentage protein density continues to increase in T47-D cells between 4-8 hours, there is a percentage decrease of HIF-1α protein in MCF-7 cells.

3.1.5 Development of Western Blot Assay for, and Analysis of, Changes in GREB1, PS2 and CASC4 Protein Expression in Response to HIF-1α stabilisation in Breast Cancer Cell Lines.

Based on our analysis of the ChIP-seq data for ERα binding in response to DMOG we identified three gene loci, *GREB1, PS2* and *CASC4* that showed changes in proximal binding. To test our hypothesis that this binding would lead to altered protein expression we undertook a western blot time course for all three proteins.

3.1.6 Evaluation of Antibodies and Membrane Types for Detection of GREB1 in Breast Cancer Cell Lines

We evaluated the performance of GREB1 antibody from Abcam (Ab72999) and two commonly used membrane types, PVDF and nitrocellulose, to determine the optimal reagents for the assay for our GREB1 time course. We conducted western blot analysis on cell lysates from MCF-7 breast cancer cells using the different antibody and membrane combinations. Our results revealed significant differences in GREB1 expression between each cell line. Nitrocellulose membrane outperformed PVDF membrane in terms of sensitivity and resolution. In addition, we compared blocking buffers: 4% milk and 3% BSA, and found no difference in the two reagents, therefore chose to continue with 4% milk. Our findings suggest that the selection of the antibody and membrane is critical for achieving accurate and reliable results in the GREB1 assay. The optimised reagents identified in this study can facilitate further investigation of GREB1's role in breast cancer and other related fields.

3.1.7 Evaluation of Antibodies and Membrane Types for Detection of PS2 in Breast Cancer Cell Lines

We evaluated the performance of PS2 antibody from Abcam (ab92377) with the same conditions as described in evaluation of GREB1 antibody above. By conducting western blot analysis using cell lysate from MCF-7 cells, found nitrocellulose membrane and 4% milk as blocking buffer to be most favourable for optimum sensitivity and resolution.

3.1.8 Evaluation of Antibodies and Membrane Types for Detection of CASC4 in Breast Cancer Cell Lines

We evaluated the performance of CASC4 antibodies from Abcam (ab230522) using western blot analysis on cell lysates from MCF-7 cancer cell lines. Our results indicated most favourable conditions being Nitrocellulose membrane, with 3% BSA blocking buffer. variations in the specificity and sensitivity of the antibodies.

3.2 Western Blot Analysis of GREB1, PS2 and CASC4 Protein in Response to HIF-1α Stabilisation in Breast Cancer Cell Lines

3.2.1 GREB1 Protein Expression Increases within 2 hours when MCF-7 and T47-D Cells are Treated with 2mM DMOG.

Utilising the timescales established by our HIF-1α time-course in MCF-7 and T47-D cells, we hypothesise that stabilisation of HIF-1α would result in detectable changes in GREB1 expression in 24 hours of treatment with DMOG. Utilising the antibodies and assay we had established, we undertook the analysis of GREB1 expression at 0, 2, 4, 8, 17 and 24 hours after stimulation with 2mM at DMOG in in MCF-7 and T47-D cells (Figure 6a (i)). GAPDH was used as the loading control and to normalise the protein density values.

In MCF-7 cells, GREB1 protein density peaks after 8 hours of incubation with DMOG. There is a general trend of increasing GREB1 protein in MCF-7 cells when HIF-1α is activated; however, the effect is not conclusive due the high variability in the result. In contrast, in T47-D cells, GREB1 protein density greatly increases after 2 hours of incubation with DMOG. After 2 hours, GREB1 protein density starts to gradually decrease, before a rapid decrease between 8 and 17 hours of incubation with DMOG. These results displayed in figure 6a (i) below, suggest that the regulation of GREB1 expression in response to hypoxic stimuli is cell type-specific and may have implications for breast cancer progression; with both cell lines showing an increase within 2 hours of stimulation of DMOG; however, analysis of expression beyond that point was less consistent between cell lines and gave no

conclusive result. The result is contradicting our hypothesis which predicted no change in GREB1 expression as no change in ER binding was at the *GREB1* genomic locus.

3.2.2 PS2, Protein Expression is Increased when MCF-7 Cells are Treated with 2mM DMOG

In MCF-7 cells, there is a fluctuating gradual increase of PS2 protein after 0 hours with all subsequent time points showing greater band density (figure 6a (ii)); however, due to the small effect size it is unclear if the result is of biological significance. The result could not be replicated in T47-D cells as there was no detectable PS2 protein at any time point confounding interpretation. Our results by western blotting therefore do not appear to support our hypothesis, based on our ChIP-seq analysis, that PS2 expression would decrease on HIF1α with DMOG.

3.2.3 Changes in CASC4 Protein Expression when MCF-7 and T47-D Cells are Treated with 2mM DMOG are Inconclusive

In MCF-7 cells, band density analysis for the CASC4 protein was higher at all time point post treatment with DMOG. After 8 hours, there is a gradual decrease, but the overall expression remains higher that pre-treatment . While the result in MCF-7 is in line with our hypothesis from the ChIP-seq data, which was generated in the MCF-7 cell line, the result could not be replicated in T47-D cells, suggesting either the result is not generalisable across cell lines or that the effect is not significant.

(i)

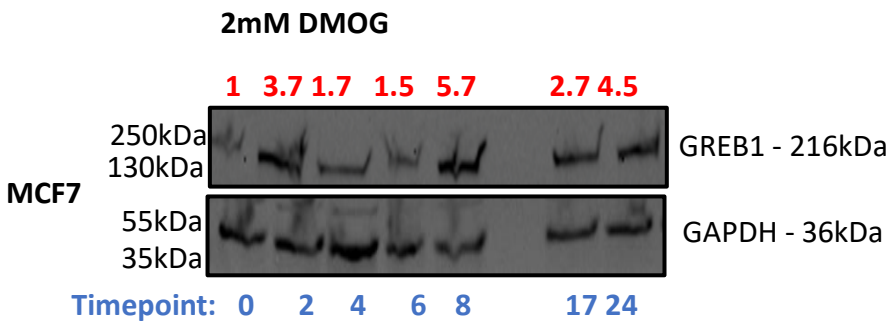
2mM DMOG
1 3.7 1.7 1.5 5.7 2.7 4.5
250kDa
130kDa
MCF7
55kDa
35kDa
GREB1 - 216kDa
GAPDH - 36kDa
Timepoint: 0 2 4 6 8 17 24

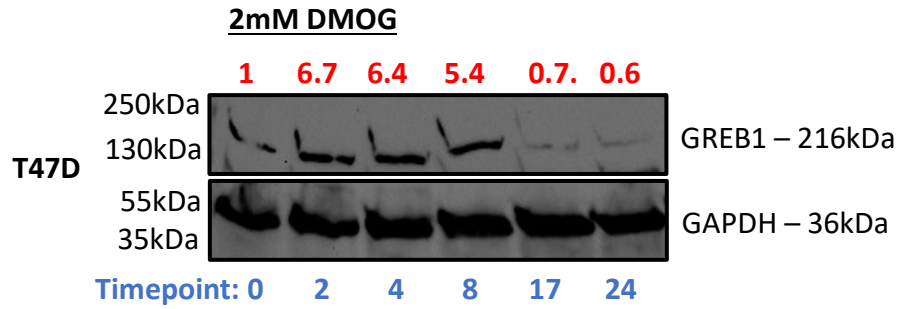
2mM DMOG
1 6.7 6.4 5.4 0.7. 0.6
250kDa
130kDa
T47D
55kDa
35kDa
GREB1 – 216kDa
GAPDH – 36kDa
Timepoint: 0 2 4 8 17 24

ii

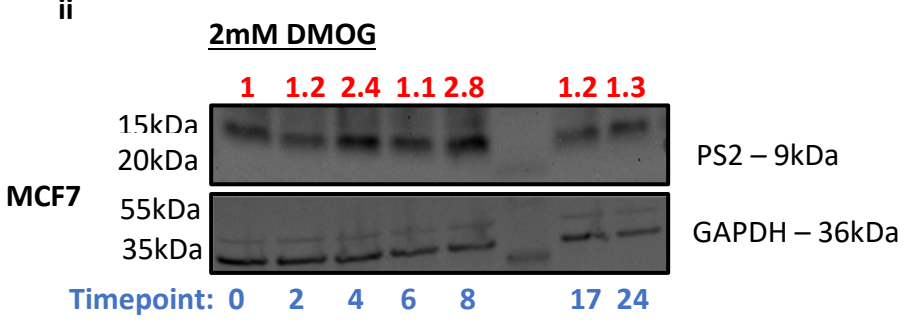
2mM DMOG
1 1.2 2.4 1.1 2.8 1.2 1.3
15kDa
20kDa
MCF7
55kDa
35kDa
PS2 – 9kDa
GAPDH – 36kDa
Timepoint: 0 2 4 6 8 17 24

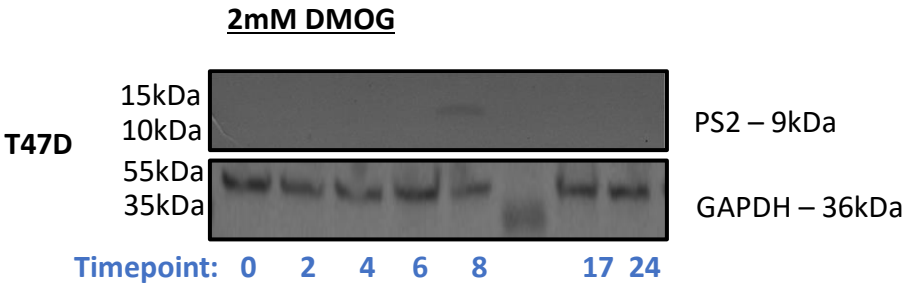
2mM DMOG
15kDa
10kDa
T47D
55kDa
35kDa
PS2 – 9kDa
GAPDH – 36kDa
Timepoint: 0 2 4 6 8 17 24

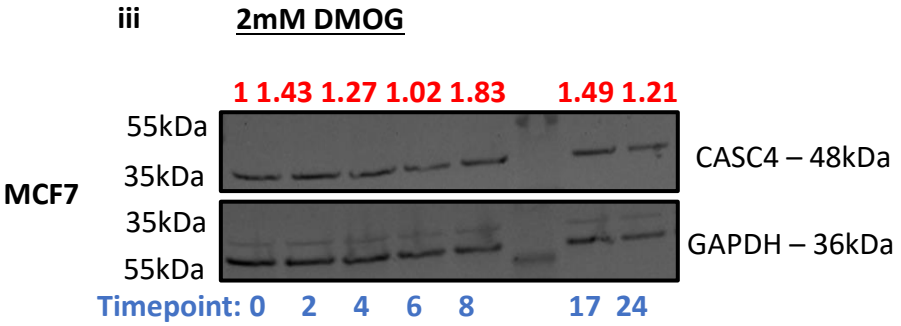

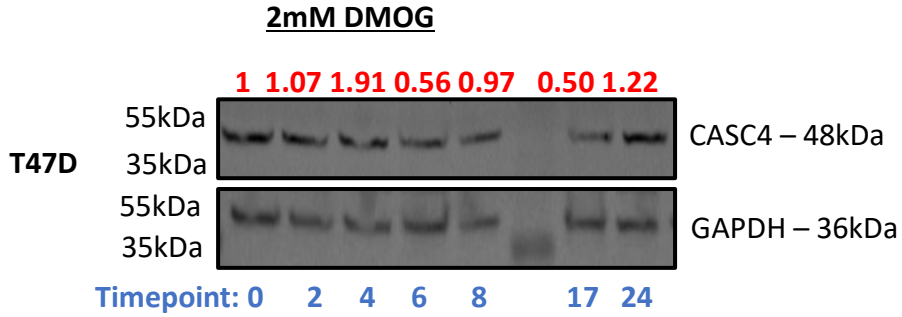

.

Figure 6a - A series of GREB1, PS2 and CASC4 western blot images displaying a time course of 2mM DMOG incubation in MCF-7 and T47-D cells.

For each time course, MCF-7 and T47-D cell lines were treated with 2mM DMOG for time points ranging from 0-24 hours. Each protein band, in each lane of the above images represents a different time point, which can be seen below the images in blue text. Protein bands were identified by their molecular weight: GREB1 (figure 6a i) 216kDa, PS2 (Figure 6a ii) 9kDa and CASC4 (figure 6a, iii) 48kDa. Below each image depicting bands of the target protein, is an image produced subsequentially of the same membrane, re-probed with GAPDH (36kDa) as a loading control. Each image underwent image analysis using ImageJ, to determine protein density values, which can be seen above each target protein band in red text.

Upper figure 6a (i), shows an increase in GREB1 protein, following 8 hours of incubation with DMOG in MCF-7 cells. Overall, throughout the 24-hour time course there is a fluctuating increase of GREB1 protein in MCF-7 cells when HIF-1α is stabilised. As we expected to see no change in GREB1 protein upon HIF-1α stabilisation, experimental error here cannot be ruled out. Lower figure 6a (i), In T47-D cells, GREB1 protein density peaks after 2 hours of incubation with DMOG. After 2 hours, GREB1 protein density starts to gradually decrease, before a rapid decrease after 8 hours of incubation with DMOG. Figure 6a (ii), in the upper image showing MCF-7 time course, there is a fluctuating gradual increase of PS2 protein between 0-8 hours, thereafter, PS2 protein density starts to decrease. No PS2 protein was detected in T47-D cells. Figure 6a (iii), the upper image showing MCF-7 time-course, CASC4 protein peaks after 8 hours of incubation with DMOG. After 8 hours, there is a gradual decrease. Comparing to GREB1 and PS2, CASC4 is the most stable protein in MCF-7 cells following HIF-1α activation because the values fluctuate less. Figure 6a (iii), lower image shows that in T47-D cells, CASC4 peaks after 4 hours of incubation with DMOG, before a gradual decrease in the protein between 4-17 hours.

3.3 Analysis of *GREB1, PS2* and *CASC4* Transcript by RT-qPCR Shows Alter Expression in Response to HIF-1α stabilisation in MCF-7 and T47-D Cells

To establish the effect of reprogramming ERα by HIF-1α stabilisation on the transcription of *PS2*, *GREB1* and *CASC4*, we quantified the abundance of mRNA transcripts in MCF-7 and T47-D cells exposure to 2mM DMOG for 17 hours by RT-qPCR. (See figure 7 below).

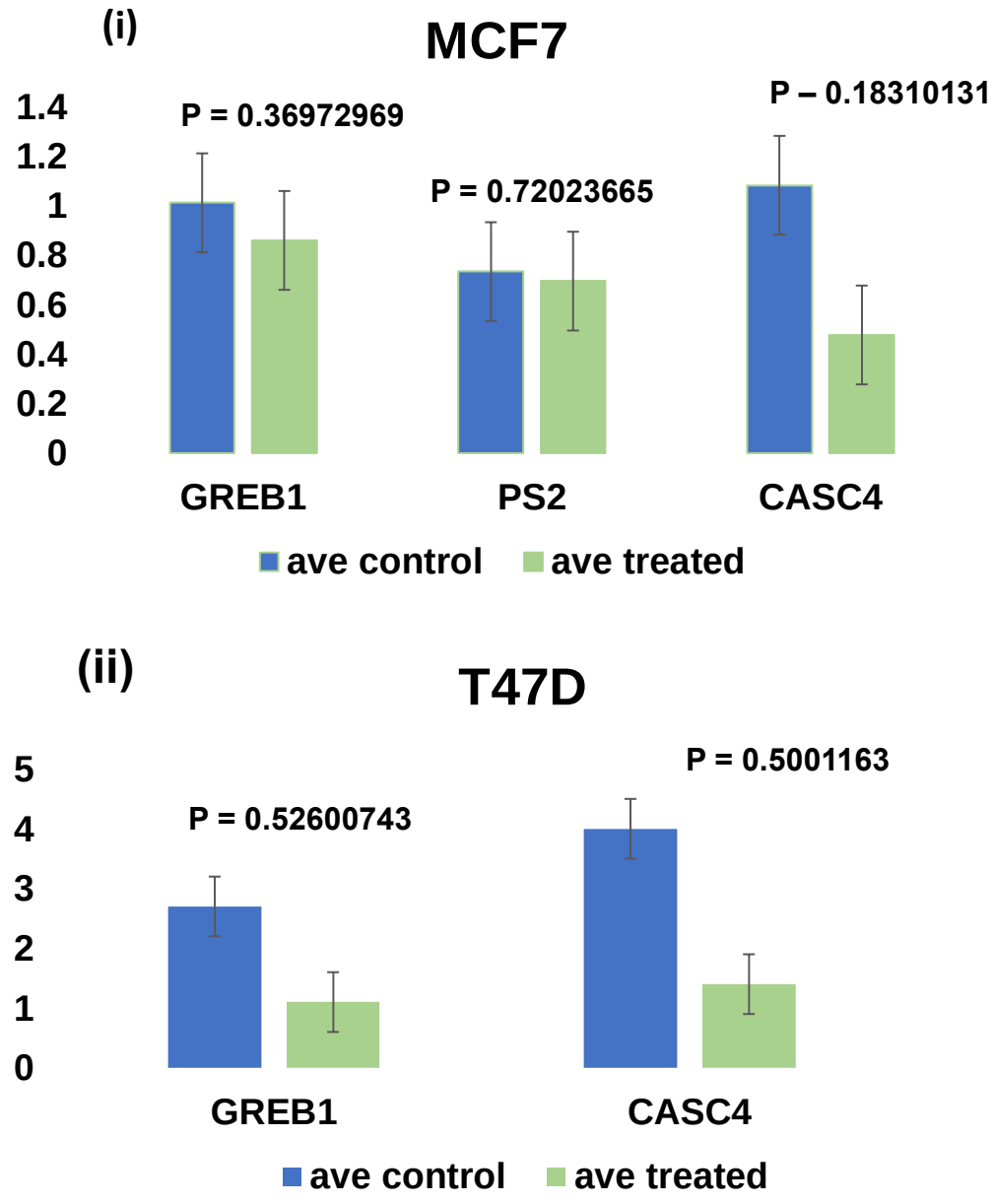

Figure 7 - Average ΔΔCt values from 3 technical repeats of GREB1, PS2 and CASC4 cells on MCF-7 and T47-D cell lines.

The above bar chart depicts results from my qPCR analysis of the transcriptional changes between GREB1, PS2 and CASC4 in response to treatment with 2mM DMOG. Error bars represent one standard deviation values of each treatment condition. Paired t-test = $p \leq 0.05$, n=3.

The results from in figure 7 were compared with qualitative analysis of western blot time course for protein products of the same genes. We hoped to gain insight from this analysis into the variability of the western blots results to either confirm if the variability was also found at the transcript level or as we expected, limited to the protein level.

HIF-1α caused a decrease in *GREB1* mRNA in MCF-7 cells, although this result is not significant. whereas in T47-D cells there is a significant decrease in *GREB1* mRNA in 2mM DMOG treated cells compared to non-treated cells. In contrast, ChIP-seq data previously acquired by the Holding lab (figure 3a/b), saw no difference in *GREB1* mRNA when MCF-7 cells were treated with 2mM DMOG compared to not treated (figure 3b (i)). Therefore, data presented here in figure 7 does not support our hypothesis from ChIP-Seq data which predicted no change in *GREB1* mRNA. However, seeing a significant increase in *GREB1* mRNA in response to HIF-1α stabilisation by DMOG, does couple with results from western blot analysis (figure 6a i) which may suggest a decrease in GREB1 protein in response to DMOG.

HIF-1α causes no significant difference in *PS2* mRNA in MCF-7 cells. ChIP-seq data (figure 3b (ii)), saw a decrease in *PS2* mRNA in MCF-7 cells that were treated with

2mM DMOG. Therefore, the results here showing no change in *PS2* mRNA expression in response to HIF-1α stabilisation does not support our initial hypothesis which suggests an increase in *PS2* in response to HIF-1α stabilisation.

There is a significant decrease of *CASC4* mRNA in MCF-7 and T47-D cells that have been treated with 2mM DMOG. This does not correlate with the ChIP-Seq data (figure 3b (iii)).

GREB1 and *PS2* data indicate transcriptional differences between MCF-7 and T47-D cells. It is therefore possible that HIF-1α stabilisation causes a different impact on MCF-7 mRNA than T47-D.

3.4 No Significant Change was Detected by PLA for the Interaction of ERα and HIF-1α Following DMOG Treatment

PLAs are a technique can detect protein-protein interaction with within 40nm (Alam., 2018). We applied this method to ascertain whether ERα and HIF-1α were within proximity of 40nm of each other within MCF-7 and T47-D cells after treatment with 2mM DMOG for 17 hours. Our analysis of confocal images detected no statistically significant result for analysis or comparison between treatment and control groups. Qualitatively reviewing the data suggests that there was a technical issue with the assay and that with further optimisations more confidence in the result could be obtained.

3.4.1 Antibody Validation Implications

Single recognition PLA (srPLA) was performed to validate the primary antibodies. Three concentrations of each antibody were tested using the two treatment conditions (2mM DMOG or DMSO as vehicle control) (see table 2). 5 images were taken using the Confocal LSM780 (Zeiss). The concentration that revealed the least background in the images was chosen for subsequent dual recognition PLA.

Table 2: Primary antibody concentrations and species used in PLA.

Antibody	Species	Concentration 1	Concentration 2	Concentration 3
HIF-1α (AB51608)	Rabbit	1/250	1/500	1/750
HIF-1α (NB100 105SS)	Mouse	1/050	1/100	1/200
ERα (AB3575)	Rabbit	1/200	1/400	1/600
ERα (8002)	Mouse	1/100	1/250	1/500

Antibody conditions that provided clean signal with low background produced by sr PLA were chosen for dual recognition PLA (dr PLA). Dr PLA was performed to investigate whether there was a protein-protein interaction between HIF-1α and ERα in MCF-7 cell lines. The experimental conditions that were set up are as follows: HIF-1α mouse/rabbit, ERα mouse/rabbit and HIF-1α rabbit with ERα mouse, with each antibody combination investigated with and without DMOG treatment.

Images were analysed and quantified using imageJ. The average number of dots/ nuclei was organised into a bar chart. Error bars which represented standard deviation, showed no significant result. Images which depicted our negative controls where no PLA signal should appear, showed some PLA signal. Therefore, any signal that appeared in our experimental control ERα/ HIF-1α was ruled out as a genuine ERα/HIF-1α protein-protein interaction. PLA depends highly on quality and specificity of the primary antibodies. As both ERα rabbit and ERα mouse which were chosen for this assay had previously been validated in the Holding lab prior to these assays, we looked to validate an alternative HIF-1α mouse antibody from Abcam. See table 3 below for antibody information.

Table 3: HIF-1α antibody concentrations and species.

Antibody	Species	Concentration 1	Concentration 2
HIF-1α (Ab1)	Mouse	1/100	1/200

A second dr PLA was performed in MCF-7 cell-lines, including new and previously validated antibodies. The assay was then repeated in T47-D cell lines. Although there was visibly more PLA signal in the HIF-1α/ERα mouse condition with 2mM DMOG than DMSO, error bars representing standard deviation, again overlapped, deeming this an insignificant result.

High variability in the data can be attributed to only a small amount of PLA signal in the confocal imagery in the HIF-1α/ERα condition for both cell lines, the effect size is not great enough for significance. The issue at hand is the large amount of background signal picked up in the confocal imagery. Further attempts to validate the primary antibodies were not undertaken due to the available time.

4. Discussion

ER has a critical role in the growth and proliferation of 70% of breast cancer patients, and due to the protein's role as a transcription factor, it is considered a master transcription regulator of ER+ breast cancer cells (Yang et al., 2015). Our labs' previous findings showed that HIF-1α stabilisation by DMOG (Yang, Harris and Davidoff., 2018) can robustly reprogramme the ER binding to chromatin, and our hypothesis that these changes in ER binding will lead to changes in the downstream effects of estrogen signalling was the foundations for this project.

Here I present my results on the effects of HIF-1α stabilisation on three ERα target genes, both the protein and mRNA. Two of my ERα target genes, *GREB1* and *PS2* , are previously well described in the literature (Ross-Innes et al., 2012, Hodgkinson et al., 2018, Zhang et al., 2019, Buache et al., 2011) while the *CASC4* gene is less widely investigated; however, it is reported to correlate with ER/ progesterone receptor (PR) expression (Duval et al., 2020) Through the validation and application of western blot assays for these three proteins, I explored the effects of inducing a hypoxia-mimicking response pathway on the expression of all 3 proteins. In addition, RT-qPCR analysis allowed me to explore the expression of all 3 ERα targets at the mRNA level.

4.1 MCF-7 and T47-D cell lines are fundamental tools for breast cancer research

To ensure the results generated by this project could build upon our labs' preliminary findings (figure 3a/b) I initially undertook all protein and mRNA analysis using the MCF-7 cell line as a model of ER+ breast cancer. This choice was to ensure that my results matched the conditions used for the generation of our labs' ERα ChIP-Seq data.

While cell lines present limitations in their ability to model disease e.g., absence of immune cell, not always accurately replicating primary tissues, and typically grown in 2D culture, they are cost effective, proliferate indefinitely and are generally more robust than primary cells, making them a suitable model for initial investigation into cancer biology (Salinas-Vera et al., 2022). Using cell lines also allowed us to mimic the *in vivo* effects of HIF-1α stabilisation on ER+ breast cancer.

To ensure biological reproducibility and confirm that our results was generalisable beyond a single ER+ breast cancer model, I then supplemented my results using T47-D cell lines (Salinas-Vera et al., 2022). Both cell lines are model of the luminal A breast cancer cells due to their abundance of ERα expression, and absence of overexpression of the HER2 receptor. For these reasons, MCF-7 and T47-D cell lines are comparable to most hormone responsive, invasive breast cancers (Yu et al., 2017, Lee, Oesterreich and Davidson., 2015) and have been used extensively for cell line models for breast cancer research.

4.1.1 DMOG Successfully Stabilises HIF-1α in MCF-7 and T47-D Cells to Mimic the Short-Term Hypoxic Response

Previous assessment of the timing of HIF-1α stabilisation in MCF-7 cells, via the inhibition of HIF prolylhydroxylases by DMOG, did not capture changes of expression at less than 24 hours after treatment (Jarman et al., 2019). At 24 hours HIF-1α is fully stabilised, therefore, I applied my western blot assays to the analysis of HIF-1α in MCF-7 and T47-D cells over a time-course of 0-24 hours after treatment with the inhibitor. The inhibition of PHD initially mimics the short-term hypoxic response in both MCF-7 and T47-D cells after hours of DMOG treatment (figure 5a), confirming the accumulation of HIF-1α protein is very rapid and occurs much faster than 24 hours. The peak in HIF-1α protein abundance (between 4-8 hours), in both cell lines, is followed by a subsequent decline. These results are in line with previously reported results in other tissues (Jing et al., 2019), as prolonged hypoxic stress leases to the reduction of HIF-1α protein, followed by the increase in HIF-2a which regulates the chronic hypoxic response (Jarman et al., 2019). Overall, we see that HIF-1α abundance peaks between 4-8 hours in MCF-7 and T47-D cells following 2mM DMOG treatment. With knowledge of which time-point with DMOG incubation accumulated the most HIF-1α protein in MCF-7 and T47-D cells, a time course of 2–24 hours for the for the analysis of GREB1, CASC4 and PS2 protein expression was performed.

4.2 Gene Products were Selected for Western Blot Analysis and RT-qPCR Analysis on the Basis of Changes in ER Binding as Detected by ChIP-seq

From analysis of our previous ER ChIP-Seq data, showing that the genomic locations of ER binding is dramatically and robustly altered in response to HIF1α activation, we identified *GREB1, PS2* and *CASC4* as three genes near to genomic locations that represented the range of responses in ER binding in response to HIF-1α activation. The range of responses are: unchanged, lost and gained binding respectively. Western blot analysis over 2-24 hours allowed us to explore whether these changes in ER binding at these gene loci were reflected at a protein level (figure 6a). On the basis that established ER function of activating gene proximal to the proteins binding, I hypothesise that with HIF-1α stabilisation in ER+ breast cancer cells, HIF-1α interacts with ERα, to increase ER binding, either by altering chromatin accessibility creating new ER binding sites, or by HIF-1α recruiting ER to new loci via protein-protein interaction, and that these changes in ER binding would directly correlate with changes in protein expression.

4.2.1 Abundance of GREB1 Protein Appears to Initially Increase with HIF-1α Stabilisation by DMOG

By western blot, we see an immediate increase in GREB1 protein at 2 hours following HIF-1α stabilisation in both cell lines. The expression then remains higher than initial level in both cell lines until it is followed by a sharp drop in expression at 17 hours in T47D which is not replicated in MCF-7 cells. Overall, the detection of protein expression is highly variable between time-points in each cell line making further interpretation difficult. Further elaboration of this potential finding, that GREB1 protein expression increases following HIF-1α stabilisation is not possible at this point. Results cannot be conclusive without further technical repeats with subsequent statistical analysis. Despite western blot analysis being a very common assay, and that my work has established a robust assay for GREB1 protein detection within the available time, there are limitations in the assay in terms of reproducibility.

Despite these limitations, it seems likely that my hypothesis that GREB1 expression would be unaltered by the stabilisation of HIF-1α is incorrect. As GREB1 is a known facilitator of the transcription of ER target genes (Stute et al., 2012), and itself is a ER target gene. Further exploration of these changes in GREB1 protein in ER+ breast cancer cells in response to HIF-1α activation are of significant interest.

4.2.2 Abundance of PS2 Protein appears to Increase with HIF-1α Stabilisation by DMOG

Western blot analysis shows an unexpected increase in PS2 protein in MCF-7 cell lines following HIF-1α stabilisation. This increase is gradual within the first 2 hours of the time-course but starts to increase more rapidly between 2-8 hours, before a gradual decrease. This result was not replicated in T47-D cells as no PS2 protein was detected in this cell lines. As an ER+ breast cancer cell line, T47-D cells are known to express PS2 protein (Buache et al., 2011) therefore, it is apparent that further optimisation of PS2 protein for western blot analysis is required.
Contrastingly, we see a significant decrease of *PS2* mRNA in response to HIF-1α stabilisation by DMOG in MCF-7 cells by RT-qPCR analysis (figure 7). A decrease in *PS2* mRNA, supports my initial hypothesis, that PS2 is reduced in response to HIF-1α stabilisation in ER+ breast cancer cell lines. Whilst western blots and RT-qPCR both provide information about gene expression, there are inherit differences in the regulation of protein and mRNA levels within the cell. Therefore, *PS2* mRNA not directly mirroring the response that PS2 protein exhibits due to HIF-1α stabilisation is not unprecedented (Buccitelli & Selbach., 2020).

mRNA levels can be a positive indicator of gene expression, however, post-transcriptional mechanisms such as alternative splicing, miRNA-mediated mRNA degradation and mRNA stability may affect abundance of protein independently of mRNA levels (Corbett., 2018). In addition, protein degradation mechanisms can affect protein levels independently of mRNA levels such as proteasomal degradation and autophagy (Tai and Schuman,. 2008).

4.2.3 CASC4 Protein and *CASC4* mRNA response to HIF-1α is Inconclusive

Inconsistent results for CASC4 protein from western blot analysis and *CASC4* mRNA from RT-qPCR analysis, means no clear conclusion can be drawn about CASC4 response to HIF-1α stabilisation in MCF-7 and T47-D cell lines.

5. Future Direction

The overall aim of this project was to build on preliminary data by the Holding lab which reveals that an increase or decrease in ER binding in response to HIF-1α stabilisation by DMOG will result in an increase or decrease respectively of the nearby gene transcripts and protein products based on changes in ER binding. This report presents a year of research, dedicated to this aim.

The present results have provided the right conditions to further investigate GREB1, PS2 and CASC4 protein using western blot analysis. Challenges presented in this report are primarily related to the need for further optimisation with the primary antibodies chosen for this assay. Additional work is required to establish the right conditions to be able to perform a western blot analysis of PS2 protein in T47-D cell lines.

Part of this research project was dedicated to primer design, followed by optimisation for RT-qPCR assays, with the objective to quantify changes in abundance *GREB1, PS2* and *CASC4* mRNA in MCF-7 and T-47D cells when exposed to 2mM DMOG. Due to limited lab time and the balance of adjacent assays, RNA isolation and cDNA synthesis would happen on separate days. In future, more care should be made with RNA work, to reduce RNA storage time and proceed quickly with cDNA synthesis to protect the RNA integrity. Consequentially, this may produce more consistent data and improve the potential for statistically significant results.

6. Conclusion

Our lab has shown that HIF-1α stabilisation in ER+ breast cancer cell lines robustly reprogrammes the ER oncogenic signalling pathway. This project has not been able to conclude on our hypothesis that loss and/or gain in ER binding in response to HIF-1α stabilisation will result in an increase or decrease respectively of the nearby gene's transcripts and protein products based on changes in ER binding. Western blot analysis showed a potential increase in GREB1 protein in both cell lines and an increase in PS2 protein in MCF-7 cell lines, which does not support initial hypothesis derived from ChIP-Seq data. Further investigation is required for a deeper understanding of the relationship between HIF-1α and GREB1 in ER+ breast cancer cells. Changes to CASC4 on a protein and transcriptional level were inconclusive. RT-qPCR analysis of *GREB1, PS2* and *CASC4* show that mRNA alterations are cell line-specific in response to DMOG. Therefore, further investigation into how MCF-7 and T47-D cells may respond differently to HIF-1α is required. *PS2* mRNA was decreased on HIF-1α activation in both cell lines, supporting the initial hypothesis; and *CASC4* mRNA was increased on HIF-1α activation, also supporting initial hypothesis, however without further statistical analysis, we cannot confirm this as a conclusive result. Overall, a deeper mechanistic understanding of the HIF-1α ERα interaction in ER+ breast cancer cells will identify a new therapeutic target for ER+ breast cancer.

Appendix

Appendix 1.1: Tables displaying list of reagents, suppliers and product codes.

A summary of cell culture reagents:

Cell Culture		
Reagent	Supplier	Product Code
DMEM Media	Gibco	41966029
Foetal Bovine Solution 10% (FBS)	Gibco	16140-071
PBS	Sigma Aldrich	P3813
Trypsin-EDTA (0.05%), phenol red	Gibco	25300-054
MCF-7 cell-line	ATCC	N/A
T47-D cell-line	ATCC	N/A
50mg DMOG	Merck	400091
DMSO	Sigma Aldrich	D2650

A summary of reagents used to create cell lysate:

Cell Lysate		
Reagent	Supplier	Product Code
2x Laemmli Sample Buffer	Bio-Rad	64394236
PBS	Sigma Aldrich	P3813
Protease Inhibitor	Roche	11873580001
β-mercaptoethanol	Bio-Rad	1610710

Secondary antibodies:

Secondary Antibodies		
Reagent	Supplier	Product Code
secondary-HRP anti-rabbit IgG antibodies	Jackson Immuno Research	111-035-144

A summary of reagents used to perform gel electrophoresis:

Gel Electrophoresis		
Reagent	Supplier	Product Code
Mini Protean®TGX™ Precast Gels 4-20%	Bio-Rad	1610732
4–20% Mini-PROTEAN® TGX Stain-Free™ Protein Gels	Bio-Rad	4568094
10X Tris/glycine/SDS	Bio-Rad	1610732
PAGE Ruler Plus	Thermo Scientific	26619

A summary of reagents required for gel transfer:

Gel Transfer		
Reagent	Supplier	Product Code
iBlot 2 transfer stacks nitrocellulose	Bio Rad	IB23001
iBlot 2 transfer stacks PVDF	Bio Rad	IB24001

A

summary of blocking reagents:

Blocking		
Reagent	Supplier	Product Code
Milk Powder	Marvel	N/A
Bovine Serum Albumin (BSA)	Sigma Aldrich	100345075

A summary of primary antibody concentrations and compatible blocking buffer:

Antibody	product code	Concentration	Lot Number	Blocking Buffer	membrane
GREB1	ab72999	1/1000	GR3324824-1	4% Milk in PBS	NC
PS2	ab92377	1/1000	GR135537-8	4% Milk in PBS	NC
CASC4	ab230522	1/1000	GR3230232-8	3% BSA in PBS	NC
HIF-1α	361695	1/5000	36169	5% Milk in TBS	PVDF
GAPDH	10494-1-ap	1/7500	10494-1-AP	4% Milk in PBS	NC
ERα	ab3575	1/1000	GR3364872-4	4% Milk in PBS	NC

Wash buffer reagent:

Wash Buffer		
Reagent	Supplier	Product Code
10% Tween 20	Bio-Rad	1662404

Summary of reagents required for imaging:

Imaging		
Reagent	Supplier	Product Code
ECL Reagent	Pierce	32109
SuperSignal™ West Pico PLUS	Thermo Scientific	34579

A summary of reagents required for proximal ligation assay:

PLA		
Reagent	Supplier	Product Code
PBS	In House	N/A
Duolink orange starter kit (mouse/rabbit)	Sigma Aldrich-Merck	DUO92102

A summary of primary antibody dilutions for proximal ligation assay:

	PLA Antibody Dilutions				
Antibody	supplier	Species	product code	Lot #	Dilution v/v
ERα	Abcam	Rabbit	AB3575	GR3364872-4	1/400
ERα	Santa Cruz	Mouse	8002	A2021	1/250
HIF-1α	Abcam	Rabbit	AB51608	GR3266947-3	1/500
HIF-1α	Abcam	Mouse	AB1	GR3364074-5	1/75

Summary of reagents used for RNA isolation:

RNA Isolation		
Reagent	Supplier	Product Code
TRIzol ™	Invitrogen	15596026
Chloroform	Sigma Aldrich	1003337279
Isopropanol	In house	N/A
Ethanol	In house	N/A

Summary of regents required for agarose gel electrophoresis:

Agarose gel electrophoresis		
Reagent	Supplier	Product Code
Agarose	Melford	9012-36-6
1x TAE buffer	in house	N/A
Syber safe DNA gel stain	Invitrogen	533102
6x orange DNA loading dye	thermo-scientific	Rob31

Summary of reagents required for cDNA synthesis:

cDNA synthesis		
Reagnet	Supplier	Product Code
Oligo (dT)	Invitrogen	2214159
10 mM dNTP mix	Invitrogen	18427-013
5x SSIV Buffer	Invitrogen	18090010
100 mM DTT	Invitrogen	R0861
RNaseOUT™	Invitrogen	100000840
Superscript™IV RT	Invitrogen	18090010
0.1M DTT	Invitrogen	18090010

Master mix reagent:

Mastermix		
Reagnet	Supplier	Product Code
(2x) fast SYBR® green master mix	ThermoFisher	4385612

Summary of forward and reverse oligo sequences:

Primer Pairs	
Oligo Name	Sequence (5'-3')
GREB1 forward	GTCTCCTCTGACTTCAACAGCG
GREB1 reverse	ACCACCCTGTTGCTGTAGCCAA
CASC4 forward	CAGCATGGCTCTAAACTGGC
CASC4 reverse	AGCTCTCGTTCTTCATCATCTTG
PS2 forward	GCCTTTGGAGCAGAGAGGAG
PS2 reverse	TGGAGGGACGTCGATGGTAT
GAPDH forward	GGATTTGGTCGTATTGGG
GAPDH reverse	GGAAGATGGTGATGGGATT

Summary of thermal cycling conditions required for RT-qPCR:

Instrument	Step	Temperature℃	Duration	Cycles
● step 1. ● Step One plus. ● 7500 fast.	AmpliTaq® fast DNA polymerase, UP activation	95	20 sec	HOLD
	Denature	95	3 sec	40
	Anneal/Extend	60	30 sec	

Appendix 1.2 Supplementary Figures:

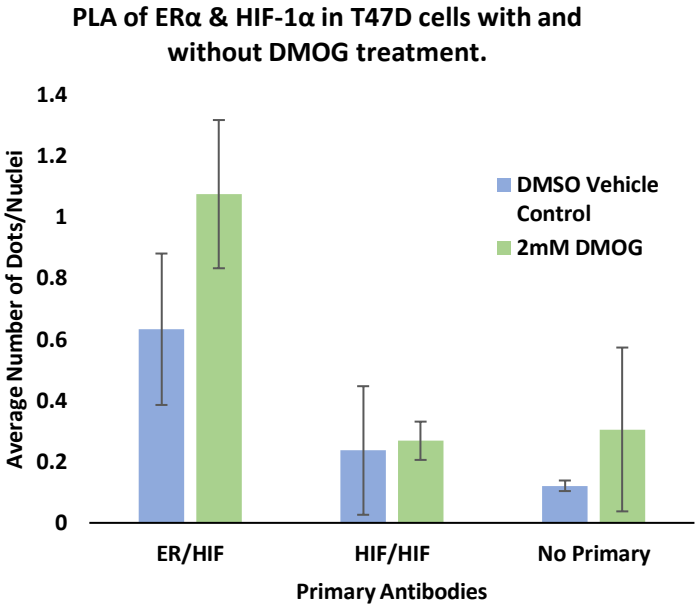

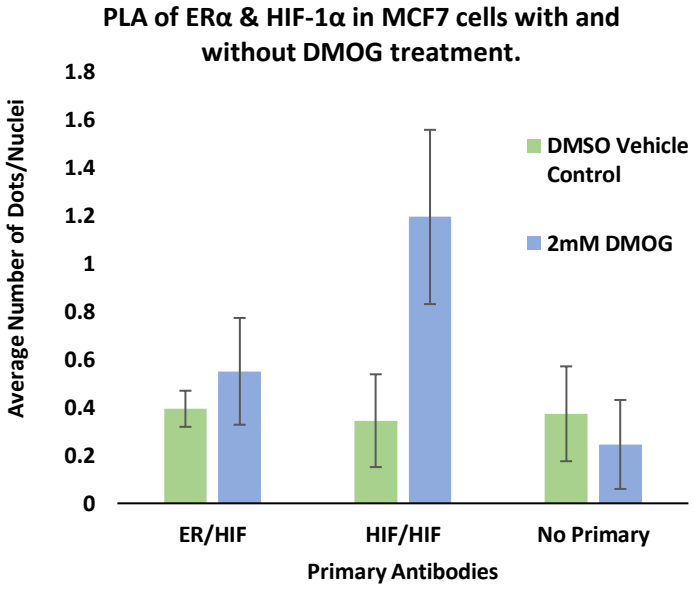

Bar charts to show average number of dots/nuclei in T47-D cells (top bar chart), MCF-7 cells (bottom bar chart) following confocal image analysis using ImageJ.

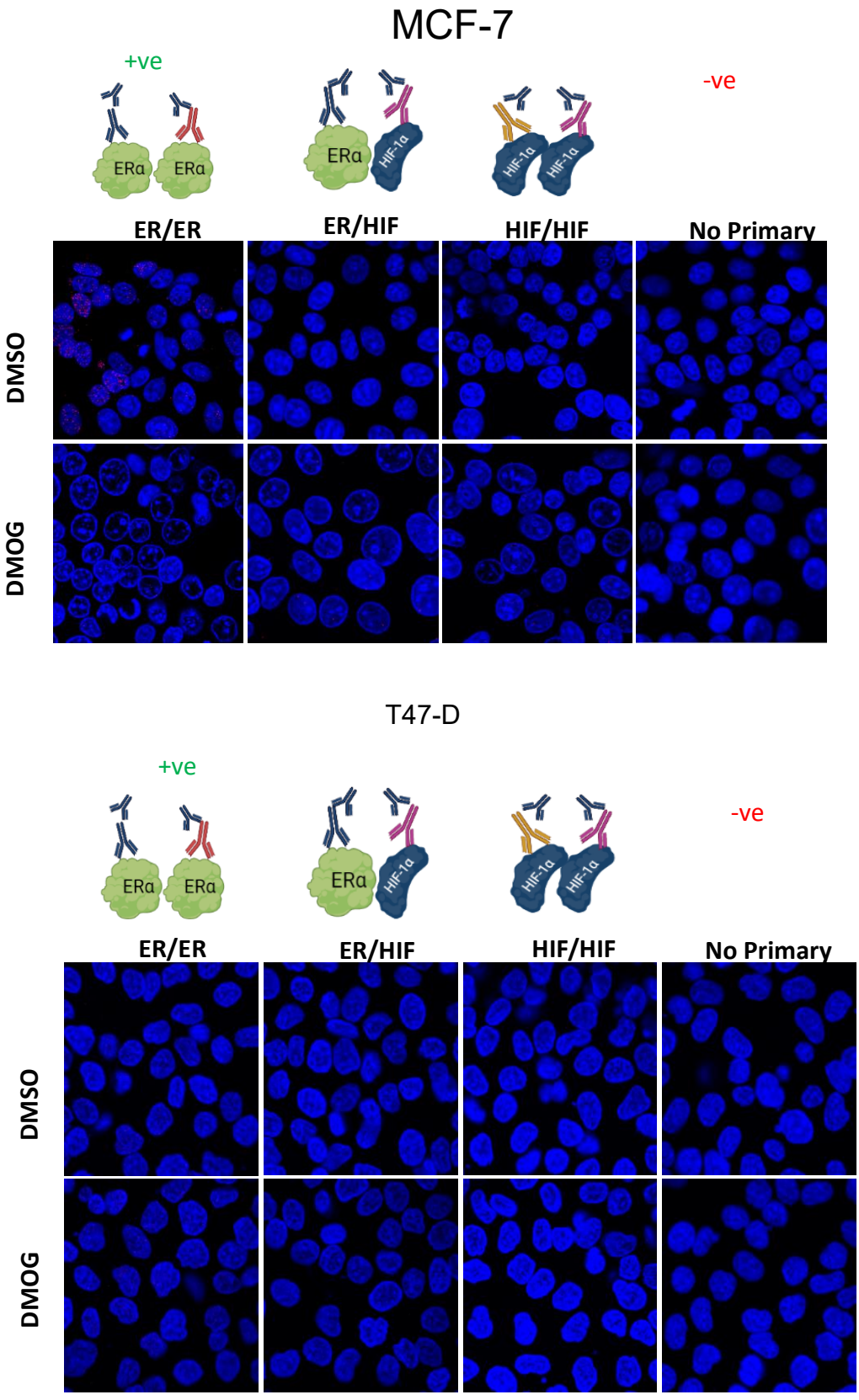

Confocal imaging of MCF-7 cells (top) T47-D cells (bottom). With graphics to represent dual recognition PLA.

7. References

Alva, R. et al. (2022). Supraphysiological Oxygen Levels in Mammalian Cell Culture: Current State and Future Perspectives. *Cells*, 11 (19), MDPI. [Online]. Available at: doi:10.3390/cells11193123.

Azzi, S., Hebda, J. K. and Gavard, J. (2013). Vascular permeability and drug delivery in cancers. *Frontiers in Oncology*, 3 AUG. [Online]. Available at: doi:10.3389/fonc.2013.00211.

Bardia, A. et al. (2019). EMERALD: Phase III trial of elacestrant (RAD1901) vs endocrine therapy for previously treated ER+ advanced breast cancer. *Future Oncology*, 15 (28), Future Medicine Ltd., pp.3209–3218. [Online]. Available at: doi:10.2217/fon-2019-0370.

Buache, E. et al. (2011). Deficiency in trefoil factor 1 (TFF1) increases tumorigenicity of human breast cancer cells and mammary tumor development in TFF1-knockout mice. *Oncogene*, 30 (29), pp.3261–3273. [Online]. Available at: doi:10.1038/onc.2011.41.

Corbett, A. H. (2018). Post-transcriptional regulation of gene expression and human disease. *Current Opinion in Cell Biology*, 52, Elsevier Ltd., pp.96–104. [Online]. Available at: doi:10.1016/j.ceb.2018.02.011.

Duval, S. et al. (2020). Shedding of cancer susceptibility candidate 4 by the convertases PC7/furin unravels a novel secretory protein implicated in cancer progression. *Cell Death and Disease*, 11 (8). [Online]. Available at: doi:10.1038/s41419-020-02893-0.

Fuentes, N. and Silveyra, P. (2019). Estrogen receptor signaling mechanisms. In: *Advances in Protein Chemistry and Structural Biology*. 116. Academic Press Inc. pp.135–170. [Online]. Available at: doi:10.1016/bs.apcsb.2019.01.001.

Hanker, A. B., Sudhan, D. R. and Arteaga, C. L. (2020). Overcoming Endocrine Resistance in Breast Cancer. *Cancer Cell*, 37 (4), Cell Press., pp.496–513. [Online]. Available at: doi:10.1016/j.ccell.2020.03.009.

Hodgkinson, K. et al. (2018). GREB1 is an estrogen receptor-regulated tumour promoter that is frequently expressed in ovarian cancer. *Oncogene*, 37 (44), pp.5873–5886. [Online]. Available at: doi:10.1038/s41388-018-0377-y.

Jarman, E. J. et al. (2019). HER2 regulates HIF-2α and drives an increased hypoxic response in breast cancer. *Breast Cancer Research*, 21 (1). [Online]. Available at: doi:10.1186/s13058-019-1097-0.

Jing, X. et al. (2019). Role of hypoxia in cancer therapy by regulating the tumor microenvironment. *Molecular Cancer*, 18 (1), BioMed Central Ltd. [Online]. Available at: doi:10.1186/s12943-019-1089-9.

Pecorino. (2021). *Molecular biology of cancer: mechanisms, targets and theraputics* . fifth edition. Oxford University Press.

Lee, A. V., Oesterreich, S. and Davidson, N. E. (2015). MCF-7 Cells - Changing the Course of Breast Cancer Research and Care for 45 Years. *Journal of the National Cancer Institute*, 107 (7), Oxford University Press. [Online]. Available at: doi:10.1093/jnci/djv073.

Lee, P., Chandel, N. S. and Simon, M. C. (2020). Cellular adaptation to hypoxia through hypoxia inducible factors and beyond. *Nature Reviews Molecular Cell*

Biology, 21 (5), Nature Research., pp.268–283. [Online]. Available at: doi:10.1038/s41580-020-0227-y.

Lee, S. H., Golinska, M. and Griffiths, J. R. (2021). Hif-1-independent mechanisms regulating metabolic adaptation in hypoxic cancer cells. *Cells*, 10 (9), MDPI. [Online]. Available at: doi:10.3390/cells10092371.

Liang, H. et al. (2018). Hypoxia induces MIR-153 through the IRE1α-XBP1 pathway to fine tune the HIF1α/VEGFA axis in breast cancer angiogenesis. *Oncogene*, 37 (15), pp.1961–1975. [Online]. Available at: doi:10.1038/s41388-017-0089-8.

Liberti, M. V. and Locasale, J. W. (2016). The Warburg Effect: How Does it Benefit Cancer Cells? *Trends in Biochemical Sciences*, 41 (3), Elsevier Ltd., pp.211–218. [Online]. Available at: doi:10.1016/j.tibs.2015.12.001.

Liu, Z. ji, Semenza, G. L. and Zhang, H. feng. (2015). Hypoxia-inducible factor 1 and breast cancer metastasis. *Journal of Zhejiang University: Science B*, 16 (1), Zhejiang University Press., pp.32–43. [Online]. Available at: doi:10.1631/jzus.B1400221.

Maity, A. et al. (2001). Low pO 2 2 2 and β β β-estradiol induce VEGF in MCF-7 and MCF-7-5C cells: relationship to in vivo hypoxia. *Breast Cancer Research and Treatment*, 67.

Masoud, G. N. and Li, W. (2015a). HIF-1α pathway: Role, regulation and intervention for cancer therapy. *Acta Pharmaceutica Sinica B*, 5 (5), Chinese Academy of Medical Sciences., pp.378–389. [Online]. Available at: doi:10.1016/j.apsb.2015.05.007.

Mishra, A. et al. (2021). Metabolic reprograming confers tamoxifen resistance in breast cancer. *Chemico-Biological Interactions*, 347, Elsevier Ireland Ltd. [Online]. Available at: doi:10.1016/j.cbi.2021.109602.

Nathan, M. R. and Schmid, P. (2017). A Review of Fulvestrant in Breast Cancer. *Oncology and Therapy*, 5 (1), pp.17–29. [Online]. Available at: doi:10.1007/s40487-017-0046-2.

Pereira, E. R. et al. (2014). Endoplasmic Reticulum (ER) stress and Hypoxia response pathways interact to Potentiate Hypoxia-inducible Factor 1 (HIF-1) Transcriptional activity on targets like Vascular Endothelial Growth Factor (VEGF). *Journal of Biological Chemistry*, 289 (6), pp.3352–3364. [Online]. Available at: doi:10.1074/jbc.M113.507194.

Rashid, M. et al. (2021). Up-down regulation of HIF-1α in cancer progression. *Gene*, 798, p.145796. [Online]. Available at: doi:10.1016/J.GENE.2021.145796 [Accessed 11 November 2022].

Reinert, T. et al. (2018). Endocrine therapy for ER-positive/HER2-negative metastatic breast cancer. *Chinese Clinical Oncology*, 7 (3). [Online]. Available at: doi:10.21037/cco.2018.06.06.

Roig, E. M. et al. (2019). HIF-1α and HIF-2alpha; differently regulate the radiation sensitivity of NSCLC cells. *Cells*, 8 (1). [Online]. Available at: doi:10.3390/cells8010045.

Ross-Innes, C. S. et al. (2012). Differential oestrogen receptor binding is associated with clinical outcome in breast cancer. *Nature*, 481 (7381), pp.389–393. [Online]. Available at: doi:10.1038/nature10730.

Ruohola, J. K. et al. (1999b). Vascular endothelial growth factors are differentially regulated by steroid hormones and antiestrogens in breast cancer cells. *Molecular and Cellular Endocrinology*, 149.

Salinas-Vera, Y. M. et al. (2022). Three-Dimensional 3D Culture Models in Gynecological and Breast Cancer Research. *Frontiers in Oncology*, 12, Frontiers Media S.A. [Online]. Available at: doi:10.3389/fonc.2022.826113.

Schaaf, M. B., Garg, A. D. and Agostinis, P. (2018). Defining the role of the tumor vasculature in antitumor immunity and immunotherapy article. *Cell Death and Disease*, 9 (2), Nature Publishing Group. [Online]. Available at: doi:10.1038/s41419-017-0061-0.

Schödel, J. et al. (2011). High-resolution genome-wide mapping of HIF-binding sites by ChIP-seq. *Blood*, 117 (23). [Online]. Available at: doi:10.1182/blood-2010-10-314427.

Semenza, G. L. (2012). Hypoxia-inducible factors in physiology and medicine. *Cell*, 148 (3), Elsevier B.V., pp.399–408. [Online]. Available at: doi:10.1016/j.cell.2012.01.021.

Semenza, G. L. (2013). HIF-1 mediates metabolic responses to intratumoral hypoxia and oncogenic mutations. *Journal of Clinical Investigation*, 123 (9), pp.3664–3671. [Online]. Available at: doi:10.1172/JCI67230.

Sestak, I. et al. (2018). Comparison of the performance of 6 prognostic signatures for estrogen receptor–positive breast cancer a secondary analysis of a randomized clinical trial. *JAMA Oncology*, 4 (4), pp.545–553. [Online]. Available at: doi:10.1001/jamaoncol.2017.5524.

Smythies, J. A. et al. (2019). Inherent DNA -binding specificities of the HIF -1α and HIF -2α transcription factors in chromatin. *EMBO reports*, 20 (1). [Online]. Available at: doi:10.15252/embr.201846401.

Soni, S. and Padwad, Y. S. (2017). HIF-1 in cancer therapy: two decade long story of a transcription factor. *Acta Oncologica*, 56 (4), Taylor and Francis Ltd., pp.503–515. [Online]. Available at: doi:10.1080/0284186X.2017.1301680.

Srinivasan, S. and Dunn, J. F. (2011). Stabilization of hypoxia-inducible factor-1α in buffer containing cobalt chloride for Western blot analysis. *Analytical Biochemistry*, 416 (1), pp.120–122. [Online]. Available at: doi:10.1016/j.ab.2011.04.037.

Stute, P. et al. (2012). Life stage differences in mammary gland gene expression profile in non-human primates. *Breast Cancer Research and Treatment*, 133 (2), pp.617–634. [Online]. Available at: doi:10.1007/s10549-011-1811-9.

Tai, H. C. and Schuman, E. M. (2008). Ubiquitin, the proteasome and protein degradation in neuronal function and dysfunction. *Nature Reviews Neuroscience*, 9 (11), pp.826–838. [Online]. Available at: doi:10.1038/nrn2499.

Valko-Rokytovská, M. et al. (2021). Breast cancer: Targeting of steroid hormones in cancerogenesis and diagnostics. *International Journal of Molecular Sciences*, 22 (11), MDPI. [Online]. Available at: doi:10.3390/ijms22115878.

Wagner, J. et al. (2019). A Single-Cell Atlas of the Tumor and Immune Ecosystem of Human Breast Cancer. *Cell*, 177 (5), pp.1330-1345.e18. [Online]. Available at: doi:10.1016/j.cell.2019.03.005.

Waks, A. G. and Winer, E. P. (2019). Breast Cancer Treatment: A Review. *JAMA - Journal of the American Medical Association*, 321 (3), American Medical Association., pp.288–300. [Online]. Available at: doi:10.1001/jama.2018.19323.

Wigerup, C., Påhlman, S. and Bexell, D. (2016). Therapeutic targeting of hypoxia and hypoxia-inducible factors in cancer. *Pharmacology and Therapeutics*, 164, Elsevier Inc., pp.152–169. [Online]. Available at: doi:10.1016/j.pharmthera.2016.04.009.

Yang, J. et al. (2015). Estrogen receptor-α directly regulates the hypoxiainducible factor 1 pathway associated with antiestrogen response in breast cancer. *Proceedings of the National Academy of Sciences of the United States of America*, 112 (49), pp.15172–15177. [Online]. Available at: doi:10.1073/pnas.1422015112.

Yang, J., Harris, A. L. and Davidoff, A. M. (2018). Hypoxia and hormone-mediated pathways converge at the histone demethylase KDM4B in cancer. *International Journal of Molecular Sciences*, 19 (1), MDPI AG. [Online]. Available at: doi:10.3390/ijms19010240.

Yu, S. et al. (2017). The T47D cell line is an ideal experimental model to elucidate the progesterone-specific effects of a luminal A subtype of breast cancer. *Biochemical and Biophysical Research Communications*, 486 (3), pp.752–758. [Online]. Available at: doi:10.1016/j.bbrc.2017.03.114.

Zhang, S. et al. (2015). *Stabilization of Hypoxia-inducible Factor by DMOG Inhibits Development of Chronic Hypoxia-Induced Right Ventricular Remodeling*. [Online]. Available at: www.jcvp.org.

Zhang, Y. et al. (2019). The expression and role of trefoil factors in human tumors. *Translational Cancer Research*, 8 (4), AME Publishing Company., pp.1609–1617. [Online]. Available at: doi:10.21037/tcr.2019.07.48.